Miner Deposita (2018) 53:665–682
DOI 10.1007/s00126-017-0766-0

ARTICLE

Multiphase formation of the Obří důl polymetallic skarn deposit, West Sudetes, Bohemian Massif: geochemistry and Re–Os dating of sulfide mineralization

František Veselovský[1] · Lukáš Ackerman[1,2] · Jan Pašava[1] · Karel Žák[2] · Eva Haluzová[2] · Robert A. Creaser[3] · Petr Dobeš[1] · Vojtěch Erban[1] · Radko Tásler[4]

Received: 16 May 2017 / Accepted: 25 September 2017 / Published online: 18 October 2017

Abstract The Obří důl Fe–Cu–As polymetallic sulfide skarn deposit is developed in a metamorphic series in the West Sudetes, Bohemian Massif. It consists of lenses of marble, calc–silicate rocks, and skarns. We studied the Gustav orebody, which is located few hundred meters away from the contact with a large, late-orogenic Variscan Krkonoše–Jizera Plutonic Complex (KJPC) emplaced into shallow crust. Mineralogical and fluid inclusion study evidence indicates that the main sulfide stage, dominated by pyrrhotite, arsenopyrite, and chalcopyrite originated from aqueous hydrothermal fluids with salinity up to 8 wt% NaCl eq. with minimum homogenization temperatures ranging from 324 to 358 °C. These fluids mainly replaced carbonate-rich lithologies. Carbon, oxygen, and strontium isotope data in Ca-rich rocks imply total overprinting by channelized metasomatic fluid flow, which is most probably related to the intrusion of the KJPC, whereas $\delta^{34}S$ values of sulfides argue for a magmatic source of sulfur. The Re–Os age of arsenopyrite overlaps published age data for the KJPC and suggests synchronous formation of the main sulfide mineralization and pluton emplacement.

Keywords Bohemian Massif · Polymetallic skarn deposit · West Sudetes · Arsenopyrite · Re–Os geochronology

Editorial handling: B. Lehmann

Electronic supplementary material The online version of this article (https://doi.org/10.1007/s00126-017-0766-0) contains supplementary material, which is available to authorized users.

✉ Lukáš Ackerman
ackerman@gli.cas.cz

[1] Czech Geological Survey, Geologická 6, 152 00 Praha 5, Czech Republic

[2] Institute of Geology of the Czech Academy of Sciences, Rozvojová 269, 165 00 Praha 6, Czech Republic

[3] Department of Earth and Atmospheric Sciences, University of Alberta, Edmonton, AB T6G 2R3, Canada

[4] Czech Speleological Society, ZO 5-02, Albeřice, Stará Alej 462, 542 24 Svoboda nad Úpou, Czech Republic

Introduction

Given the wide original definition of the term skarn (mineral paragenesis containing calcium-bearing silicates derived from limestone or dolomite with the introduction of variable amounts of Si, Fe, and other elements; e.g., Holmes 1920), a range of various mineral deposits has been classified as skarn in the past. In ore deposit research, the term skarn was frequently used only for skarn sensu stricto, i.e., metasomatic (replacement) mineral assemblages spatially and temporally related to granitic intrusions with a generally iron-rich mixture of coarse-grained Ca–Mg–Fe–Al silicates (typically garnet and pyroxene, but usually without feldspar), formed at relatively high temperature (e.g., Einaudi and Burt 1982; Meinert 1992; Meinert et al. 2005). Modern metamorphic rock reviews similarly defined skarn as a metasomatic rock (e.g., Fettes and Desmonds 2007). A typical feature of skarns is their pronounced spatial, mineralogical, and chemical zonation, observable at most deposits.

Skarns are often associated with exploitable accumulations of ore minerals of a wide range of metals—Fe, Cu, Zn, Pb, Mo, Sn, W, As, and Au. The presence of these components defines up to seven geochemically distinct skarn types, each usually associated with a different major/trace element composition of associated plutonic rock (Einaudi et al. 1981; Einaudi and Burt 1982; Meinert et al. 2005). Another classification subdivides skarns depending on the composition of

the original rock to those derived from calcic limestone, dolomite, and silicate rocks (skarns derived from silicate rock are usually dominated by scapolite). The other types of calc–silicate rocks formed by a wide variety of processes including regional metamorphism, but without the widespread metasomatism by external fluids, would be classified as calc–silicate hornfels (usually fine-grained rocks) or calc–silicate bands (erlans in the Central European terminology).

The traditionally wide usage of the term skarn is also reflected in the geological literature focusing on the Bohemian Massif (easternmost part of the Variscan orogen in Europe). The term was used in its paragenetic sense, i.e., typically for rocks dominated by garnet (grossular–andradite) and clinopyroxene (diopside–hedenbergite), commonly with magnetite and other ore minerals formed typically at the contact with associated granitic rocks (e.g., Mikulski and Speczik 2016), and sometimes overprinted by retrograde processes leading to emergence of amphiboles and epidote. Since the rocks in the Bohemian Massif with skarn assemblages are usually regionally metamorphosed (in greenschist, amphibolite or eclogite facies), a continuing discussion exists on the nature of their pre-metamorphic equivalents. One or more metamorphic events superimposed on the original mineral assemblage (including also the retrograde metamorphism) enhance the complexity of the problem, since metamorphic overprint modifies the textures and chemical and mineralogical composition of the skarns (e.g., Meinert et al. 2005 and references therein).

At present, there are two main views on the origin of skarns of the Bohemian Massif: (1) formation by high-temperature metasomatism followed by Variscan regional metamorphism (e.g., Reh 1932; Koutek 1950; Němec 1964; Šrein and Šreinová 2000; Žáček 2007; Bubal 2013; Bubal and Dolejš 2013) or (2) origin by metamorphism of sedimentary Fe-rich horizons or sedimentary exhalative ore deposits (SEDEX) suggested especially for magnetite-rich types (e.g., Klomínský and Sattran 1963; Pertold and Pouba 1982; Pertold et al. 1997; Drahota et al. 2005; Pertoldová et al. 2014 and references therein). The post-metamorphic high-temperature metasomatism related to intrusion of late-orogenic Variscan granitoids is not considered to be the dominant process of skarn formation in the Bohemian Massif. Nevertheless, in several cases, the formation of at least the sulfides (Fe–Cu–As) was assumed to be related to these granitoids (e.g., Klomínský and Sattran 1963; Novák 1964; Hoth and Lorenc 1966; Mochnacka et al. 2015; Mikulski and Speczik 2016).

The availability of advanced dating methods, like Re–Os dating of base–metal sulfides (e.g., Stein et al. 2000; Morelli et al. 2007; Kerr and Selby 2011), offers a further step forward in understanding of the complex multistage processes of the ore formation. In this respect, the Obří důl skarn deposit in the Krkonoše Mts., a prominent ore deposit in northern Bohemia, was selected for a pilot study. The deposit had a leading position in the Bohemian market for As and Cu in the periods 1828–1868 and 1830–1853, respectively (Kurfiřt and Tásler 2014); further extensive underground prospection took place in 1952–1959, resulting in excellent present-day accessibility. This polymetallic Fe–Cu–As deposit is developed in a metamorphic series containing lenses of marble, calc–silicate rocks, amphibolite, and skarns in intimate contact with the large, late-orogenic Variscan Krkonoše–Jizera Plutonic Complex (KJPC).

Several contradictory ideas on the genesis of skarn mineral assemblages of the Obří důl deposit have been presented. Additionally, Obří důl is considered to some extent analogous to the Czarnów deposit (earlier known as Rothenzechen) on the Polish side of the border, for which also several genetic opinions were published (e.g., Mikulski 2010; Mochnacka et al. 2015 and references therein).

In this paper, we present new data for the Obří důl skarn deposit, which include petrography and mineralogy of the ore paragenesis, fluid inclusion studies, and stable (C–O) and Sr isotopic compositions of the skarns and their lithological precursors, accompanied by new Re–Os gechronological data on arsenopyrite.

Geological setting and the Obří důl skarn deposit

Regional geology

The Variscan Belt in Europe formed as the result of the collision of Laurussia–Baltica, Gondwana, and a number of intervening microplates such as Avalonia or Armorica during Middle to Late Paleozoic (Franke 1989). The Bohemian Massif, constituting the easternmost part of the Variscan Belt in Europe, represents one of its largest exposures. It is formally divided into four major tectonic units (Kosmatt 1927; Matte et al. 1990; Schulmann et al. 2009): (i) Saxothuringian Unit, (ii) Teplá–Barrandian Unit, (iii) Moldanubian Unit, and (iv) Moravo–Silesian Unit.

The Obří důl skarn deposit is located in the Saxothuringian Unit, which contains a variable spectrum of low- to high-grade metamorphic rocks such as gneiss, orthogneiss, mica schist, and quartzite (Kemnitz et al. 2002; Linnemann and Romer 2002; Linnemann et al. 2008a; Kröner and Romer 2010). The lithological, geochemical, and isotope characteristic of the protoliths are relatively uniform (Linnemann et al. 2008a), generally related to geotectonic processes during the Cadomian and Variscan orogenic cycles. The Cadomian volcanosedimentary complex with maximum age of ~ 570 Ma is characterized by diverse tectonostratigraphic history (Linnemann and Romer 2002; Buschmann et al. 2006; Linnemann et al. 2007) and intrusions of voluminous granitoids at ~ 540–530 Ma forming the large Lusatia Granitoid

Complex (Kröner et al. 1994; Linnemann et al. 2000; Tichomirova 2002; Białek et al. 2014) accompanied by small granitic bodies (Glasbach, Laubach; Linnemann et al. 2000; Buschmann et al. 2001; Linnemann et al. 2004). During Variscan time, the Saxothuringian Zone became one of the most complex parts of the Variscan Belt in Central Europe (Franke 1995). Two main domains with different evolution can be distinguished: (i) Erzgebirge Crystalline Complex, which consists of at least five tectonometamorphic units with complex evolution (Klápová et al. 1998; Linnemann et al. 2008b; Mazur et al. 2015) intruded by composite granitic plutons at 325–318 Ma (Breiter et al. 1999; Romer et al. 2007 and references therein) with composition ranging from primitive S-types to highly evolved A-types, and (ii) Western-Central Sudetes (Lusatian Unit) representing a complex of various volcanosedimentary units with different tectonic history accompanied by intrusion of four major composite plutons making up the Sudetic Granite Belt (Finger et al. 2009), which include the Krkonoše–Jizera Plutonic Complex (KJPC).

The KJPC (or Karkonosze Granite; Fig. 1) is the largest exposed granite massif in the Sudetes (Mazur et al. 2007; Kryza et al. 2014). It is situated in the center of the dome-shaped Krkonoše–Jizera Crystalline Complex/Terrane (Kachlík and Patočka 1998; Hladil et al. 2003) also called Karkonosze–Izera Massif in the Polish geological literature (Aleksandrowski and Mazur 2002; Kryza et al. 2014). It consists of five different facies (Borkowska 1966; Žák and Klomínský 2007; Žák et al. 2013; Kryza et al. 2014): (1) the most widespread I-type biotite granite (the Liberec and Jizera type) and (2) medium-grained equigranular biotite granite (the Harrachov type). These two facies form the majority of the KJPC; the other types are subordinate: (3) medium-grained two-mica granite of S-type (the Tanvald type) of local extent on the SW margin of the KJPC, (4) amphibole–biotite diorite to granodiorite (the Fojtka type), and (5) granophyric granite, which is poorly exposed within the porphyritic facies in the NE part of the KJPC. Large lamprophyre dyke swarms were described from the eastern and western parts of the KJPC (Awdankiewicz 2007; Žák and Klomínský 2007). Ages for the KJPC cover a relatively large interval. The structurally deeper western part of the KJPC yields ages from 320.1 ± 3.0 to 315.0 ± 2.7 Ma (U–Pb zircon LA–ICP–MS; Žák et al. 2013) whereas younger ages 312.5 ± 0.3 and 312.2 ± 0.3 Ma have been determined for the upper, central-eastern part of the KJPC closer to the studied area (U–Pb zircon CA–ID–TIMS; Kryza et al. 2014). The dome-shaped metamorphic envelope of the KJPC is represented by the Cambrian or Lower Ordovician Izera–Kowary Unit (Oberc-Dziedzic et al. 2010). It was subdivided into Jizera orthogneisses and mica schists on the northern side (Fig. 1) and the South Krkonoše Metamorphic Complex (Winchester et al. 2003) formed mainly by mica schist with minor intercalations of amphibolite, quartzite, marble, calc–silicate rocks, and skarns and Krkonoše orthogneiss (Marheine et al. 1999).

The Izera–Kowary Unit hosts two main types of skarn deposits: (1) magnetite skarns (e.g., Herlíkovice or Kowary; Mochnacka and Pošmourný 1981; Mochnacka et al. 2015) and (2) polymetallic sulfide-rich skarns, usually with higher Cu contents (e.g., Obří důl; Pašava et al. 2016b; Nové Město pod Smrkem; Pouba and Sattran 1966) or Czarnów (Mochnacka et al. 2009). While the magnetite skarns occur mainly in the "exocontact" of the orthogneiss bodies, the latter seem to exhibit spatial relationship to the KJPC contact and the presence of marbles and calc–silicate rock lenses. Skarn bodies replaced mainly the carbonate-rich rocks, but minor metasomatic replacement and formation of sulfide phases is commonly observed also in paragneisses and quartzites. The relationships are frequently modified by later tectonic processes, which also affected the ore deposits.

The Obří důl skarn deposit

The Obří důl skarn deposit (Chrt and Bolduan 1966; Mochnacka and Pošmourný 1981; Pošmourný 1982; Tásler 2012; Kurfiřt and Tásler 2014; Pašava et al. 2016a, b) is hosted by the Izera–Kowary Unit (Fig. 1) at a distance of up to a few hundred meters away from the contact of the KJPC, represented here by the common I-type porphyritic biotite granite. The deposit formed in several steps, which include regional and contact metamorphism and subsequently several hydrothermal stages related to the intrusion of the KJPC. Three known skarn orebodies within the Obří důl deposit (Helena and Gustav, and the smaller Václav orebody) differ in their geological position with respect to the contact of the KJPC and partly also in their mineralogy. The whole rock sequence in the Obří důl is dissected by several roughly foliation-parallel tectonic zones representing tectonic movements after the formation of skarns and sulfide mineralization, which resulted in recrystallization of some ore minerals (e.g., pyrrhotite; Pertold and Kopecký 1979). The late tectonic mineralization phases postdating the major ore-formation period include scheelite impregnations and quartz/carbonate veins. The 1952–1959 exploration on the Obří důl skarn deposit identified ~ 100,000 tons of ore with 0.43–0.47% of W and 856,000 tons of ore with 0.41–0.43% Cu and 0.19–0.49% Sn, predominantly located in the Helena orebody.

The *Helena orebody* (not sampled in this study) is the largest one with horseshoe shape and is developed just at the contact with the KJPC. Lenses of marble (calcite and dolomite) forming the center of the body are surrounded by pyroxene (diopside–hedenbergite)–garnet (andradite) skarn with polymetallic (Fe–As–Cu) ores. Relatively younger W–Sn mineralization is present mainly in brecciated granitic rocks

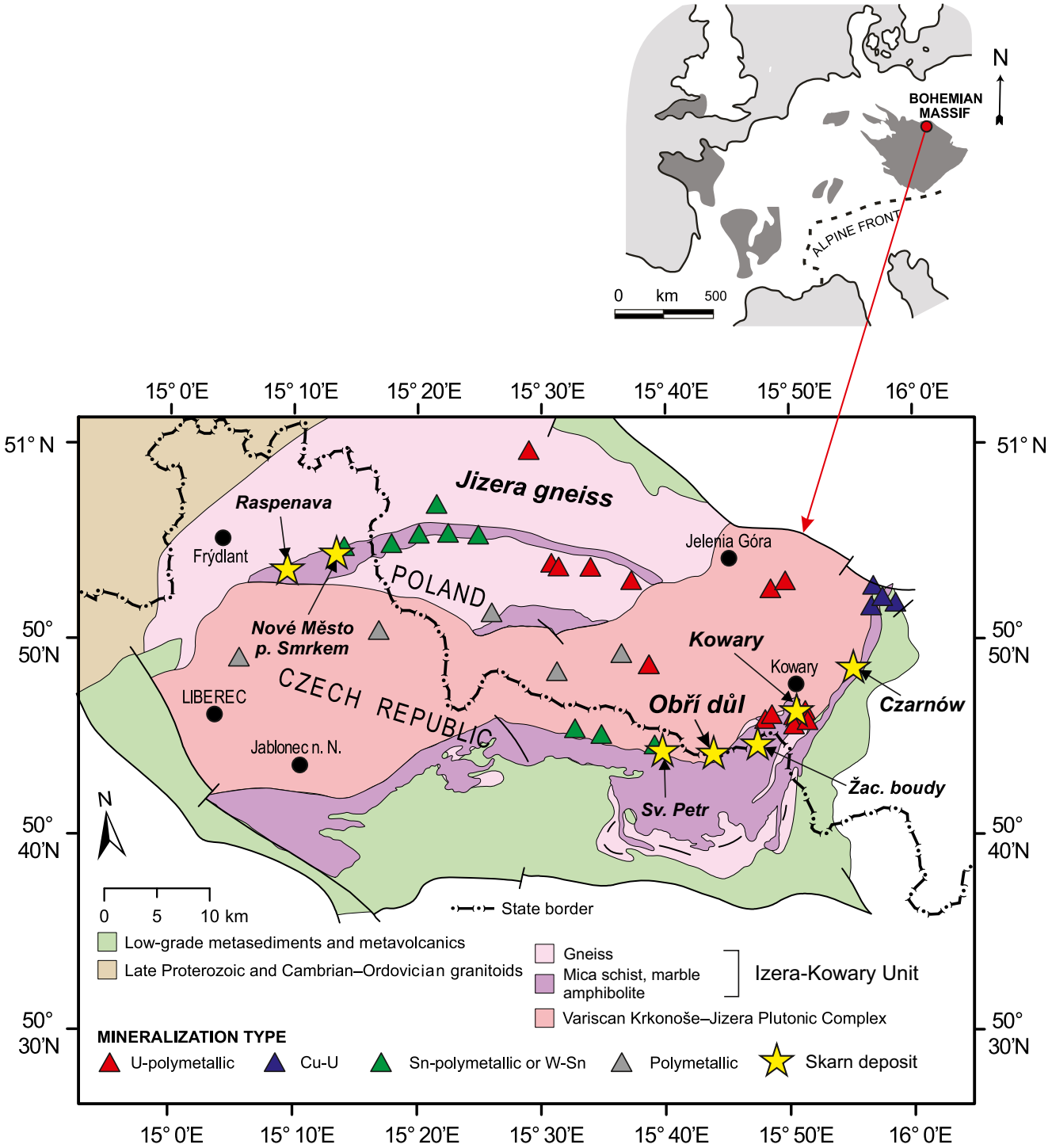

Fig. 1 Geological map of the Krkonoše–Jizera Plutonic Complex, Bohemian Massif, and related mineralization types in the Czech Republic and Poland (modified from Pašava et al. 2015)

and/or near the contact with the KJPC. The ore minerals occur as irregular clusters, impregnations, and rare veinlets and are represented by pyrrhotite, sphalerite, chalcopyrite, arsenopyrite, galena, stannite, molybdenite (all sulfides of the main sulfide stage), scheelite, cassiterite, malayite, and bismuthinite (Šrein and Šreinová 2000) .

The *Gustav orebody* (this study), located at a distance of 350–400 m from the contact with the KJPC, is developed in variegated metamorphic rocks represented by calc–silicate rocks (erlan), pyroxene (diopside)–garnet (grossular) skarn, and marble surrounded by mica schist (locally passing to orthogneiss), quartzite, and amphibolite. It has formed as an

irregular, steeply dipping (~ 80°) ore column up to 12 m thick and up to ~ 90 m in length (Fig. 2). The mineralization (Fe–As–Cu) is dominated by pyrrhotite, arsenopyrite, chalcopyrite, and minor galena occurring as replacement impregnations and/or clusters, most commonly within or in the proximity to marble (calcite-dominated) and calc–silicate rocks. Arsenopyrite was found to be the oldest sulfide mineral, and it is very likely that the dominant pyrrhotite and chalcopyrite, which replace silicates (mainly clinopyroxene), were formed contemporaneously (mostly intimately intergrown). The Gustav orebody is well-accessible through the historical Barbora adit.

The smallest *Václav orebody* (not sampled in this study) is located at the largest distance from the KJPC contact, and it is represented by rocks and mineralizations similar to the Gustav orebody.

Samples and methods

All studied samples were collected from the Gustav orebody (50.7279 N, 15.7312 E, altitude of the current mine entrance—Barbora adit—is 1014 m a.s.l.), i.e., the only part of the deposit easily accessible in the underground galleries and shafts of the historical heritage mine (Fig. 2). The sampling focused on Fe–As–Cu sulfide mineralization and rocks with carbonate for the C, O, and Sr isotope study.

The polished sections containing sulfide ores were first studied using an optical microscope and a FE–SEM Tescan Mira3 GMU, both housed at the Czech Geological Survey. Subsequently, selected mineral phases were analyzed by CAMECA SX 100 electron microprobe in the Joint Laboratory of Electron Microscopy and Microanalysis of the Czech Geological Survey and the Masaryk University. Quantitative analyses were performed using a wavelength dispersive spectrometry with accelerating voltage of 25 kV, beam current 20 nA, and beam diameter of 1 μm. Following standards were used to assess analytical precision and accuracy: Fe Kα (FeS_2), Zn Kα (ZnS), Co Kα (Co), Ni Kα (pararammelsbergite), Cu Ka (Cu), Mn Kα (Mn), As Lβ (pararammelsbergite), Se Lβ (PbSe), S Kα (FeS_2), Cd Lβ (CdTe), In Lα (InAs), Pb Mα (PbSe), Ag Lα (Ag), Bi Mβ (Bi), and Sb Lβ (Sb).

Bulk mineralogy of the rock samples was studied using a Bruker D8 DISCOVER X-ray diffraction system and software DIFFRAC.EVA with database ICDD PDF2 in the labs of the Institute of Geology of the Czech Academy of Sciences.

Fluid inclusions (FI) were studied in double-polished sections 0.3 mm thick by the methods of optical microthermometry using a Chaixmeca heating and freezing stage (Poty et al. 1976) in the laboratories of the Czech Geological Survey. The apparatus was calibrated for temperatures between − 100 and + 400 °C using chemical standards Merck, water-ice melting temperature, and by phase transitions in FI containing pure CO_2. The homogenization and cryometric data were reproducible at ± 0.2 °C at temperatures below 0 °C and ± 0.3 °C at temperatures up to 500 °C. The salinity of fluids was calculated following the procedure of Bodnar and Vityk (1995), and the salt system was evaluated following Davis et al. (1990).

To access $\delta^{34}S$ isotopic data, pyrrhotite, chalcopyrite, and arsenopyrite separates were prepared by a combination of

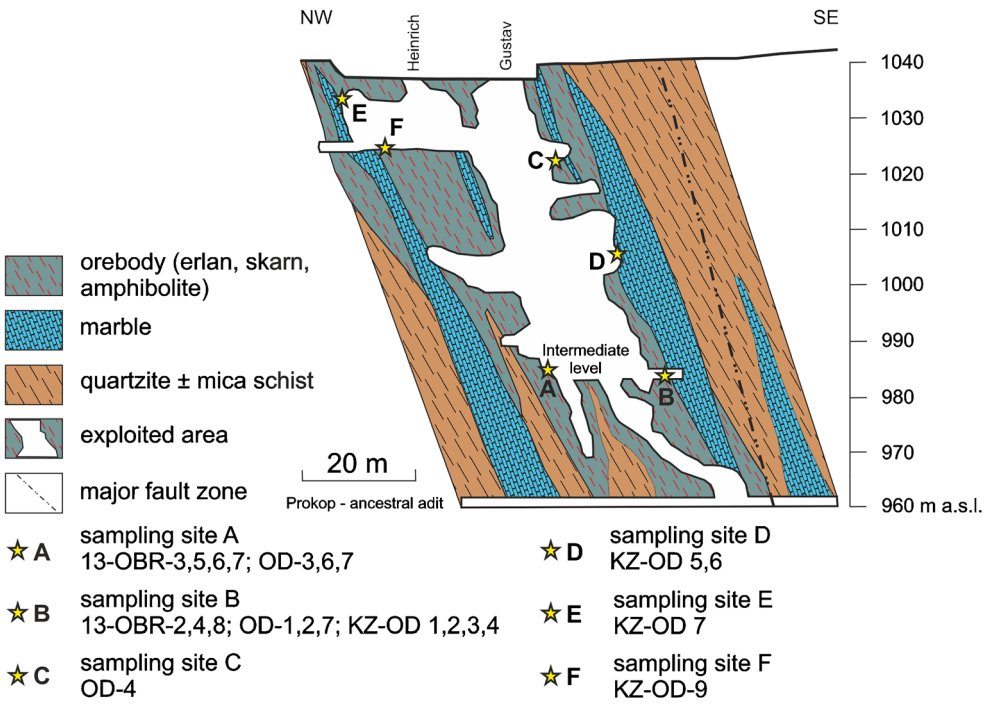

Fig. 2 Geological cross section through the Gustav orebody in the Kovárna mining area, Obří důl polymetallic skarn deposit, with sample location

hand picking from crushed specimens and physical methods (e.g., magnetic separation). The purity of mineral separates was better than 90%. Sulfur isotope compositions were determined in the Czech Geological Survey using direct oxidation by CuO under vacuum (Grinenko 1962) followed by cryogenic purification of the prepared SO_2 gas and measurement of sulfur isotope data on a Finnigan MAT 251. The overall analytical uncertainty of $\delta^{34}S$ was ± 0.3‰.

The C–O stable isotopic compositions were determined in the Czech Geological Survey using conventional carbonate decomposition by 100% H_3PO_4 under vacuum at 25 °C (McCrea 1950) followed by the measurement of the released CO_2 gas using a Finnigan Delta V mass spectrometer. The overall analytical uncertainty was ± 0.15‰ for both $\delta^{13}C$ and $\delta^{18}O$. Chemistry of the calcareous part of the samples was determined in 5% HCl leachates by ICP–OES (Agilent 5100) at the Institute of Geology of the Czech Academy of Sciences.

The Re–Os concentration and isotopic ratios for arsenopyrite were analyzed in the Crustal Re–Os Geochronology Laboratory of the University of Alberta using Re–Os isotope dilution methods described elsewhere (e.g., Morelli et al. 2010). In brief, 200–300 mg of arsenopyrite was weighed in Carius tubes, mixed with ^{185}Re–^{190}Os spike and decomposed using 2 ml of concentrated HCl and 6 ml concentrated HNO_3 at 220 °C for 24 h (Shirey and Walker 1995). Osmium was extracted from the inverse aqua regia digest solution by a combination of $CHCl_3$ and HBr, and the final fraction was purified by micro-distillation (Birck et al. 1997). Rhenium was separated by anion exchange chromatography using AG 1× 8 resin (Eichrom). Re and Os isotopic compositions were determined by N–TIMS technique (Creaser et al. 1991; Völkening et al. 1991) using a Thermo Triton instrument. Total procedural blanks for Re and Os were 0.7 and 0.4 pg, respectively. The errors stated in Table 4 include all analytical errors due to measurements, spike calibrations, weighing, etc.

Strontium was separated from samples dissolved in 5% HNO_3 using Eichrom Sr spec resin as described in Pin et al. (2014). Isotopic analyses were performed at the Czech Geological Survey with Thermo Neptune MC–ICP–MS. Calculated $^{87}Sr/^{86}Sr$ values were corrected for mass fractionation using $^{86}Sr/^{88}Sr = 0.1194$. The overall analytical uncertainty as given by repeated analyses of the NBS 987 reference material is $^{87}Sr/^{86}Sr = 0.710300 \pm 7$ (2σ; $n = 48$). Results were normalized using NBS 987 value $^{87}Sr/^{86}Sr = 0.71024$.

Results

Petrography, mineralogy, and chemistry of sulfides from the Gustav orebody

The chemical compositions of major (arsenopyrite, pyrrhotite, and chalcopyrite) and minor (pyrite, marcasite, and sphalerite) sulfide minerals together with other accessory phases (native Bi, Bi–Ag–Pb–S phases) present in the Obří důl polymetallic ores along with their description are summarized in Supplementary Tables 1 and 2, whereas ore petrography is shown in Fig. 3.

Arsenopyrite, the oldest sulfide in the paragenesis, forms both isolated idiomorphic grains and masses and clusters up to several tens of centimeters large. The grains are not homogeneous and may contain abundant, but very small inclusions of native Bi and bismuthinite (Fig. 3b). The Co content in arsenopyrite was found to be up to 0.1 wt% (Supplementary Table 1). Heterogeneity of the arsenopyrite, which can be recognized on the back-scattered images, results from the oscillation of As/S atomic ratio in the range of 0.95–1.13.

The most abundant ore minerals of the Gustav orebody are pyrrhotite and chalcopyrite, either replacing silicate minerals or carbonates (Fig. 3b). The largest accumulations reaching up to several meters in size are formed by pyrrhotite forming also networks along the silicate grain boundaries. The pyrrhotite is locally altered along fractures (Fig. 3c). The alteration product contains Fe, S, and O and seems to be homogenous even at the highest magnification. Pyrrhotite is also replaced by pyrite (Fig. 3c), which can be distinguished from pyrrhotite by a thin zone of a probably amorphous phase containing mainly Fe, Si, and O. Even the obviously fresh pyrrhotite grains show a deficit in the element sum of 1.4–4.0 wt% (Supplementary Table 1). Considering a pyrrhotite composition of $Fe_{1-x}S$, the x varies in the range of 0.12–0.16 (Supplementary Table 1). The observed range of Fe content in pyrrhotite (57.5–59.2 wt%) and sulfur (38.3–39.7 wt%) is accompanied by minor Pb admixture (0.01–0.20 wt%; Supplementary Table 1) most likely present as submicroscopic inclusions (no Pb phase was identified). The mutual relationship of pyrrhotite and chalcopyrite is difficult to observe, since both minerals usually occur in separate accumulations without a direct contact of the grains. Both minor chalcopyrite veinlets in massive pyrrhotite and younger pyrrhotite replacing chalcopyrite were rarely observed. Locally, pyrrhotite replaces chalcopyrite along fractures filled by chlorite (Fig. 3d). For the younger pyrrhotite, the x varies in a narrow range at 0.15 (Supplementary Table 1). Chalcopyrite, present mainly in the form of allotriomorphic grains, is relatively pure containing only up to 0.17 wt% of Pb. The contents of Zn and Ag are close to the detection limits (~ 0.04 wt%).

Sphalerite occurs usually together with chalcopyrite (Fig. 3d), more rarely with pyrrhotite. It contains 9.0–11.6 wt% Fe, up to 0.6 wt% Mn, 1.2–1.6 wt% Cd, and 0.8–1.6 wt% Cu (Supplementary Table 2). Other ore minerals are present only rarely. Bismuthinite [Bi_2S_3] is accompanied by native Bi and commonly contains Cd (0.3–0.6 wt%) and Zn (0.1–0.2 wt%; Supplementary Table 2). Scheelite, galena, matildite ($AgBiS_2$), and argentite (Ag_2S) were identified in the form

Table 1 Microthermometric data for fluid inclusions from the Obří důl polymetallic skarn deposit

Sample	Mineral	FI generation	FI type	LVR (L/L + V)	T_h (°C)	T_m (°C)	Salinity (wt.%)	T_{fm} (°C)	T_mCO_2 (°C)
OD-3A-1	Quartz	Primary	H_2O-(CO_2)	0.7	324–358	− 2.4 to − 5.7	4.0–8.8	− 34.2	− 58.2 to − 60.1
		Secondary	H_2O	0.8	184–210	− 5.3 to − 7.2	8.3–10.7	− 24	
OD-3A-1	Diopside	?	H_2O	0.6–0.7	387–424				
OD-3A-2	Quartz	Primary	H_2O	Variable	148–167				
OD-3A-3	Quartz	Primary	H_2O	0.5–0.95	184–390	− 2.8 to − 4.8	4.7–7.6		
OD-4	Garnet	Secondary	H_2O	Variable	236–262	− 3.1 to − 4.2	5.1–6.7		
OD-7	Calcite	Primary	H_2O	0.95	113–136	− 2.6 to − 4.6	4.3–7.3		
OD-8	Calcite	Primary	H_2O	0.9	114–154	− 0.8 to − 2.4	1.4–4.0		
		Pseudosec.	H_2O	0.9	118–134	− 0.8 to − 1.7	1.4–2.9		
13-OBR-8	Calcite	Primary	H_2O	0.9	136–168	− 2.9 to − 3.6	4.8–5.9		
		Secondary	H_2O	0.9	108–186	− 2.2 to − 2.6	3.7–4.3		
13-OBR-8	Garnet	?	H_2O	0.8	228, 242	− 4.6, − 5.3	7.3–8.3		

LVR (L/L + V) degree of fill—liquid to vapor ratio, T_h temperature of homogenization, T_m temperature of melting of the last crystal of ice, T_{fm} temperature of the first melting (eutectic temperature), T_mCO_2 temperature of melting of solid CO2

of micrometric grains whereas several small (up to 500 μm) marcasite idiomorphic grains were identified on arsenopyrite crystals. Small grains containing Bi–Pb–Ag–S (Supplementary Table 2) consist probably of at least three mineral phases, which cannot be accurately measured with respect to their extremely small size (< 1 μm). Molybdenite is a rare mineral, which is found in either skarn or granite. In granite, it forms an association with calcite, titanite, galena, native Bi, and stokesite ($CaSnSi_3O_9 \times 2\ H_2O$), which also replace molybdenite (Fig. 3e). Stokesite can be locally found also in association with pyrrhotite, cassiterite, galena, and native Bi. It was most likely formed by decomposition of cassiterite (Fig. 3f).

Fluid inclusions

Primary, pseudosecondary, and secondary fluid inclusions in different minerals (quartz, clinopyroxene, calcite, and garnet) were identified in skarns, quartz/carbonate veins, and samples with disseminated Fe–As–Cu mineralization (Supplementary Table 3 and Table 1; Fig. 4). The fluid inclusions in the major skarn minerals, clinopyroxene and garnet, were observed only

Table 2 $\delta^{34}S$ data for pyrrhotite (Po), chalcopyrite (Ccp), and arsenopyrite (Aspy) from the Gustav orebody (Obří důl polymetallic skarn deposit)

Sample no.	Description	Mineral	$\delta^{34}S$ (‰ vs. CDT)
OD-4	Massive Po (Kovárna mining area)	Po	0.9
OD-8	Massive Po (Kovárna mining area)	Po	1.2
OD-3A	Massive Po locally intergrowing with Ccp in erlan (Kovárna mining area)	Po	2.4
13-OBR-9	Massive Po with Ccp and Py (Prokop waste damp)	Po	1.1
13-OBR-5	Massive Po with Ccp and Py (Kovárna mining area)	Po	2.7
13-OBR-1	Massive Po with Ccp and Py (Kovárna mining area)	Po	1.2
13-OBR-6	Massive Po with Ccp and Py (Kovárna mining area)	Po	1.1
OD-2	Ccp in association with Po (Kovárna mining area)	Ccp	2.8
OD-2/1	Massive Ccp (Kovárna mining area)	Ccp	3.1
13-OBR-2	Massive Ccp (Kovárna mining area)	Ccp	2.7
13-OBR-3	Massive Po with Ccp (Kovárna mining area)	Ccp	3.1
OD-1	Coarse-grained Aspy locally intergrowing with Ccp (Kovárna mining area)	Aspy	4.8
OD-1/1	Coarse-grained Aspy locally intergrowing with Ccp (Kovárna mining area)	Aspy	4.1
13-OBR-4	Coarse-grained Aspy with Po (Kovárna mining area)	Aspy	4.3

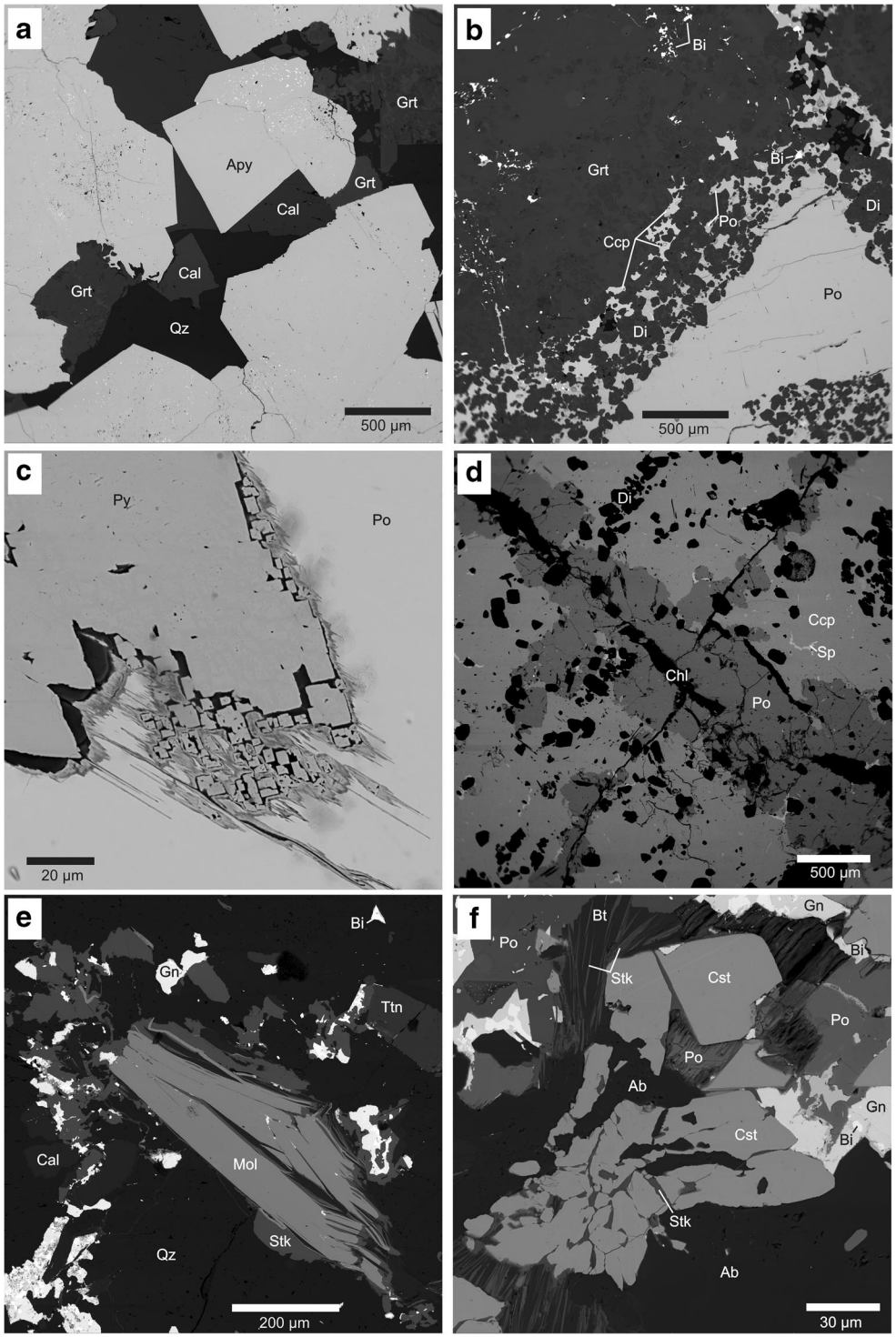

in a small number, and their parameters are therefore poorly defined. Total homogenization temperatures (to liquid in all cases) of primary inclusions largely varied among studied minerals (Table 1). Several fluid inclusions of uncertain classification in diopside have homogenization temperatures (T_h) in the range of 387–424 °C. Only secondary fluid inclusions (T_h 228–262 °C, salinity up to 8 wt% NaCl equiv.) were found in the garnet. The quartz veinlets in skarn hosting the Fe–As–Cu mineralization contain fluid inclusions with water solutions, small admixture of CO_2 and generally variable degree of fill (F) from 0.5 to 0.95 (Table 1). Temperatures of homogenization were measured in the group of inclusions with consistent degree of fill of 0.7. They yielded a narrow range of T_h 324–358 °C with salinity in the range 4.0–8.8 wt%

◀ **Fig. 3** Microphotographs of typical associations of ore minerals at the Obří důl skarn-type deposit (BSE images). **a** Euhedral grains of arsenopyrite (Apy) in association with calcite (Cal), quartz (Qz), and garnet (Grt). Arsenopyrite contains abundant very small inclusions of native Bi. **b** Gradual replacement of silicates, mainly diopside (Di) by pyrrhotite (Po) and chalcopyrite (Ccp) with chalcopyrite dominating in the front zone due to its higher mobility. Silicates (diopside—Di and garnet—Gt) often contain micro-inclusions of native Bi. **c** Replacement of pyrrhotite (Po) by pyrite (Py) with amorphous oxide matrix containing Si and Fe. Inhomogeneous phase of unknown oxi-sulfide (ferrotochiline?) replaces pyrrhotite along fractures. **d** Pyrrhotite (Po) replacing massive chalcopyrite (Ccp) along fractures locally filled by chlorite (Chl). Diopside (Di) represents residua of grains after their replacement by chalcopyrite. Sphalerite (Sp) forms inclusions in chalcopyrite (Ccp). **e** Molybdenite (Mol) in quartz gangue in association with stokesite (Stk), which locally replaces molybdenite (bottom right part of the Mo grain). Light grains are galena (Gn) often with native bismuth (Bi) and locally occurring between molybdenite grains (not shown). Calcite (Cal) and titanite (Ttn) were also identified. **f** Crushed and corroded cassiterite grains (Cst) most likely provided Sn for the formation of stokesite (Stk) which fills fractures between remnants of cassiterite grains. Stokesite is also associated with elongated biotite (Bt) grains. Pyrrhotite (Po) which forms subhedral elongated grains with apparent fissility and galena (Gn) often with native bismuth (Bi) are also part of this paragenesis

NaCl equiv. Only T_mCO_2 were observed in the inclusions. The solid CO_2 dissolved immediately, and therefore, vapor phase of CO_2 or partial homogenization of CO_2 was not observed. The admixture of CO_2 in the inclusions was very small, probably lower than 4 mol% (e.g., Roedder 1984). The T_mCO_2 values varied from − 58.2 to − 60.1 °C suggesting only a small contribution of another compound such as CH_4. The younger carbonate and quartz veinlets with no sulfide mineralization contain low saline fluids (1.4–7.3 wt% NaCl equiv., Na ± K ± Mg ± Fe chlorides) with T_h in the range 108–186 °C.

Stable (C–O–S) and Sr isotopic compositions

The sulfur isotopic compositions ($\delta^{34}S$) of pyrrhotite, chalcopyrite, and arsenopyrite from the Gustav orebody are summarized in Table 2. The observed variations are in a relatively narrow range with the lowest $\delta^{34}S$ values in the range of 0.9 to 2.7‰ found in pyrrhotite followed by slightly higher ones for chalcopyrite (2.7 to 3.1‰) and arsenopyrite (4.1 to 4.8‰).

The C and O isotopic data for carbonates from marbles, calc–silicate rocks (erlan), skarn, amphibolite, and younger veinlets are summarized in Table 3, and variability of $\delta^{18}O$ and $\delta^{13}C$ is shown in Fig. 5a. All carbonate samples in calc–silicate rocks show clear $\delta^{18}O$ and $\delta^{13}C$ shifts away from marble while the carbonates samples from the marble–erlan contact and those in skarn show a large deviation in $\delta^{13}C$ down to − 9.1‰ V-PDB at almost constant $\delta^{18}O$. Two calcite samples from younger, crosscutting veinlets exhibit diverse C and O isotope data. The carbonate from a veinlet with laumontite falls into the field of marbles (Fig. 5a) while a carbonate veinlet penetrating marble has the most negative $\delta^{18}O$ value of − 27.2‰ V-PDB.

Five samples of carbonates or the carbonate fraction from the rocks with maximum variability in $\delta^{13}C$–$\delta^{18}O$ space, which is thought to represent the metamorphic fluid variability together with degree of decarbonization, were analyzed for their $^{87}Sr/^{86}Sr$ compositions (Table 3). The obtained data roughly correlate with both C and O isotopic compositions (Fig. 5b), with the least radiogenic sample of marble having the highest $\delta^{13}C$ and $\delta^{18}O$ values, closest to the presumed marine carbonate composition (Veizer et al. 1999). In parallel, the late carbonate veinlet shows the most radiogenic $^{87}Sr/^{86}Sr$ (0.7190) in agreement with its lowest $\delta^{13}C$ and $\delta^{18}O$ values, but highest Sr content (0.05 wt%).

Re–Os isotopic compositions and geochronology

The Re–Os isotopic compositions of arsenopyrite from the Gustav orebody are given in Table 4. The samples are characterized by variable Re contents in the range between 2.3 and 25.3 ppb paralleled by very low Os from 27.5 to 94.1 ppt. Regression of these data returns a six-point Re–Os isochron with a slope yielding an age of 307.5 ± 5.6 Ma and initial $^{187}Os/^{188}Os$ value of 1.04 ± 0.33 (Fig. 6). The MSWD of 26 indicates scatter of the data beyond analytical uncertainty, and most scatter is associated with the single analysis OD-10. The remaining five analyses yield an age of 307.6 ± 4.6 Ma (MSWD = 3.0, initial $^{187}Os/^{188}Os$ = 1.11 ± 0.21.

Discussion

Ore mineralization

The observed mineral paragenesis of sulfides at the Gustav orebody is in agreement with previous studies (e.g., Šrein and Šreinová 2000 and references therein), who reported the sequence of pyrrhotite–chalcopyrite–arsenopyrite–galena–sphalerite. The oldest sulfide is arsenopyrite, and it is very likely that the dominant pyrrhotite and chalcopyrite, which replace silicates (mainly clinopyroxene), were formed contemporaneously (mostly intimately intergrown). Alteration products of pyrrhotite containing Fe, S, and O can either represent a mixture of very fine grains of Fe sulfide and Fe oxide or any iron oxy-sulfide such as a mineral phase close to ferrotochilinite ($FeS \times 0.85[Fe(OH)_2]$) (Makovicky 2006; Bernard and Hyršl 2013). The enrichment of the Obří důl polymetallic mineralization in Sn, Bi, and Ag has been confirmed by our find of stokesite, native Bi, matildite, argentite, and malayaite. Also, a recent LA–ICP–MS study of

Table 3 Results of C, O, and Sr isotope analyses in Ca-rich samples from the Gustav orebody (Kovárna mining area, the Obří důl polymetallic skarn deposit). Chemistry of calcareous part of the sample available after leaching by 5% HCl is given in wt.%

Sample no.	Type of sample	Carbonate content (wt.%)	$\delta^{13}C$ (‰ vs. V-PDB)	$\delta^{18}O$ (‰ vs. V-PDB)	$\delta^{18}O$ (‰ vs. V-SMOW)	$^{87}Sr/^{86}Sr$	Al	Ca	Fe	K	Mg	Mn	Na	P	S	Si	Sr
KZ-OD 1/1	Marble	92	−3.5	−13.9	16.6	0.70984 ± 1	0.03	36	0.13	0.06	0.36	0.03	0.06	0.03	0.04	0	0.008
KZ-OD 1/2a	Marble	84	−4.5	−15.4	15.0		0.04	33	0.07	0.09	0.64	0.07	0.11	0.01	0.08	0	0.011
KZ-OD 1/2b	Erlan	46	−5.2	−18.8	11.5		0.08	18	0.09	0.13	0.87	0.06	0.03	0.04	0.04	0	0.005
KZ-OD 1/2c	Marble	88	−4.6	−15.3	15.2		0.02	34	0.07	0.06	0.63	0.08	0.06	0.01	0	0	0.011
KZ-OD 1/2d	Erlan	52	−5.2	−18.4	12.0		0.06	20	0.07	0.24	0.51	0.06	0.13	0.06	0	0	0.006
KZ-OD 1/2e	Marble	82	−5.0	−16.0	14.5		0.03	32	0.07	0.08	0.59	0.07	0.05	0.02	0	0	0.010
KZ-OD 1/3	Marble	86	−4.6	−14.5	16.0		0.01	34	0.05	0.03	0.11	0.05	0.04	0.04	0	0	0.008
KZ-OD 2/1	Marble	90	−4.3	−16.2	14.2		0.01	35	0.05	0.08	0.48	0.05	0.09	0.01	0.1	0	0.009
KZ-OD 2/2a	Marble	78	−6.1	−21.0	9.3	0.71053 ± 1	0.02	31	0.03	0.04	0.07	0.03	0.05	0.05	0.08	0	0.008
KZ-OD 2/2b	Erlan + sulfides	28	−7.5	−20.0	10.3		0.06	11	0.19	0.08	0.27	0.06	0.07	0.09	0.08	0.244	0.003
KZ-OD 2/3	Marble	89	−3.9	−14.4	16.1		0.02	35	0.05	0.07	0.35	0.05	0.07	0.05	0.08	0	0.007
KZ-OD 3/1	Skarn	3	−9.1	−18.2	12.2		0.07	0.7	0.45	0.01	0.05	0.02	0.01	0.06	0.03	0.078	0.000
KZ-OD 5/1a	Younger veinlet	91	−8.9	−27.2	2.8	0.71902 ± 2	0.01	35	0.15	0.03	0.09	0.56	0.03	0	0.08	0	0.051
KZ-OD 5/1b	Marble	90	−4.7	−17.5	12.9	0.71196 ± 1	0.02	35	0.08	0.04	0.35	0.07	0.03	0.02	0.07	0.035	0.009
KZ-OD 6/1	Marble	89	−4.7	−13.4	17.1		0.02	35	0.05	0.05	0.08	0.03	0.04	0.03	0.03	0	0.007
KZ-OD 7/1a	Skarn contact	77	−5.4	−18.8	11.5	0.71174 ± 1	0.03	30	0.16	0.06	0.71	0.04	0.05	0.06	0.04	0.338	0.005
KZ-OD 7/1b	Skarn contact	80	−5.7	−18.5	11.8		0.03	31	0.16	0.07	0.65	0.05	0.07	0.06	0.08	0.305	0.005
KZ-OD 7/2	Marble	88	−4.2	−16.4	14.0		0.01	35	0.04	0.08	0.17	0.03	0.22	0.02	0.06	0.225	0.012
KZ-OD 8/1	Carbonate veinlet with laumontite	8	−4.8	−14.4	16.1		4.2	3.2	0.02	0.13	0.01	0	0.03	0	0.02	10.04	0.005
KZ-OD 9/1	Erlan + amphibole	9	−9.0	−25.2	4.9		0.02	3.5	0.16	0.01	0.06	0.04	0.01	0.06	0.03	0.147	0.000

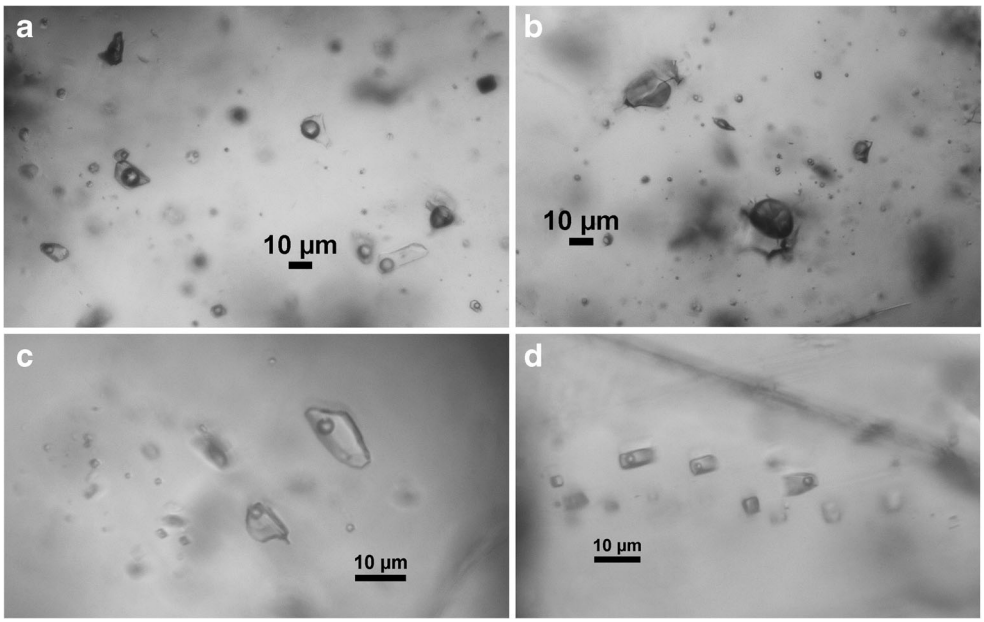

Fig. 4 Fluid inclusion types in minerals from the Obří důl skarn deposit. **a** Primary H_2O inclusions with relatively consistent LVR in quartz veinlet with sulfide mineralization (sample OD-3A), **b** primary H_2O-(CO_2) inclusions in quartz veinlet with sulfide mineralization (sample OD-3A), **c** primary H_2O inclusions with consistent LVR in calcite veinlet (sample 13-OBR-8), **d** secondary H_2O inclusions with consistent LVR in calcite veinlet (sample 13-OBR-8)

molybdenite from Obří důl (Pašava et al. 2016a) reports the presence of native Bi, galena, and inclusions of an Ag–S phase.

The Obří důl deposit shares some paragenetic and geochemical similarities with the skarn deposits (e.g., Czarnów, Kowary) located in a similar geological setting on the Polish side of the border (Mochnacka et al. 2009; Mikulski 2010) especially with respect to their multiphase origin and evolution and presence of the marble–skarn/calc–silicate rock association. The Czarnów deposit has similar mineralogy with the predominant presence of arsenopyrite–pyrrhotite in association with late-stage Sn–W mineralization (cassiterite, scheelite), which is similar to the Helena orebody from the Obří důl deposit, although the former exhibits the predominance of cassiterite over scheelite (Mikulski et al. 2007; Mochnacka et al. 2009). The Kowary deposit largely differs by the presence of large quantities of magnetite-bearing skarn and late stage U-mineralization but has a similar polymetallic sulfide paragenesis. This deposit formed in three main mineralization phases: (i) stratabound magnetite mineralization formed either due to the KJPC intrusion or by regional metamorphism of sedimentary exhalative iron mineralization and (ii) formation of skarn bodies with late-stage hydrothermal polymetallic sulfide minerals followed by (iii) uranium–polymetallic stage crosscutting the skarn (Mochnacka et al. 2015). It is also noteworthy that the whole paragenesis and chemistry of the Obří důl sulfides bears many mineralogical similarities with the high-temperature polymetallic (base metal sulfide-rich) mineralization at deposits located in high-grade metamorphic rocks in the Kutná Hora Crystalline Unit (Kutná Hora deposit) or Saxothuringian Unit (Freiberg mining district), labeled as *k-pol* mineralization type (Bernard and Pouba 1986).

Constraints from fluid inclusions

The skarn-forming fluids are typically of a wide range of composition, salinities, and temperatures (Kwak 1986; Jamtveit and Anderson 1993; Wilkinson 2001; Pašava et al. 2003). The prograde high-temperature metasomatic phase producing anhydrous silicate minerals is typically formed by hypersaline high-temperature fluids (commonly above 500 °C and salinities exceeding in some cases 50 wt% NaCl equiv. with a high content of $CaCl_2$ resulting from a reaction of NaCl-rich magmatic fluids with carbonates). The retrograde phase, which produces minerals like amphibole or epidote or assemblages with sulfides, is formed in a lower temperature interval (200–350 °C) by lower-salinity aqueous fluids with higher content of NaCl. Several fluid types of these generally wide ranges in temperature and composition were recorded in the Obří důl deposit indicating a complex evolution of associated fluids and likely long time breaks in the fluid circulation.

Fila-Wójcicka (2000) studied the petrogenesis of skarns at Garby Izerskie (NW of Szklarska Poreba, Poland) close to the KJPC contact and suggested that stage I, which took place during the prograde metamorphism in a quasi-isochemical system, resulted in crystallization of hedenbergite (ca. 500 °C) and wollastonite and grossular (ca. 600–650 °C). The latter two minerals were formed at peak metamorphic temperatures at ca. 650 °C; the fluids had a CO_2 concentration of 30 mol%. At the Obří důl skarn, only several aqueous fluid inclusions of uncertain classification in clinopyroxene had homogenization temperatures (T_h) in the range of 387–

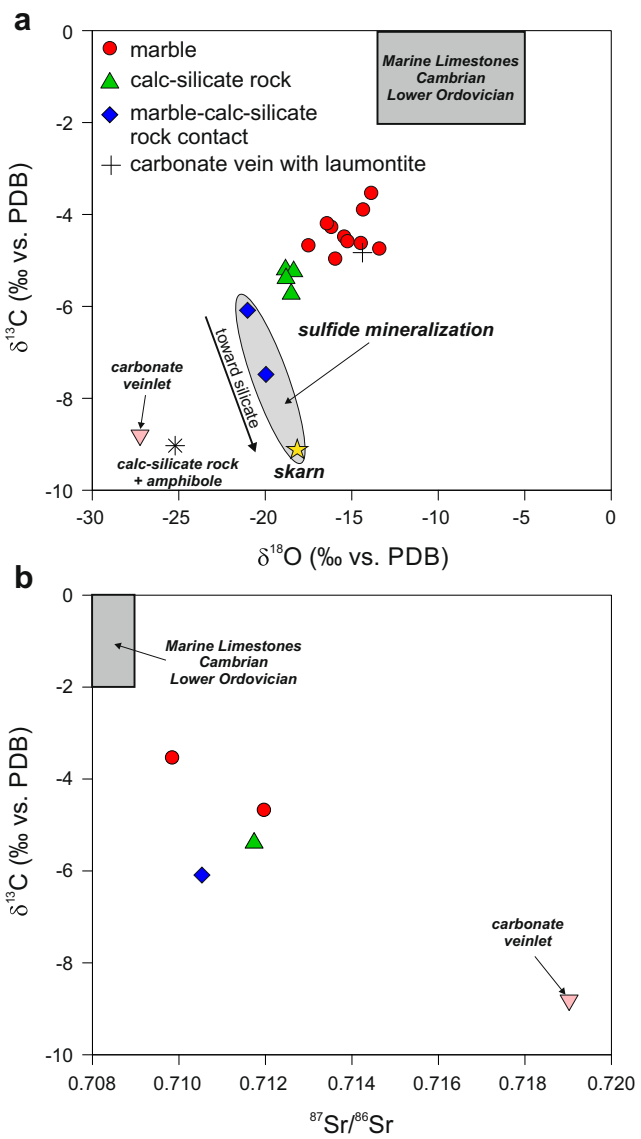

Fig. 5 **a** $\delta^{18}O$ (‰ vs. V-PDB) vs $\delta^{13}C$ (‰V-PDB) plot for Ca-rich samples from the Obří důl polymetallic skarn deposit. Field for Cambro–Ordovician marine limestone from Veizer et al. (1999). **b** $^{87}Sr/^{86}Sr$ vs. $\delta^{13}C$ (‰ vs. V-PDB). Field for Cambro–Ordovician marine limestone from Veizer et al. (1999)

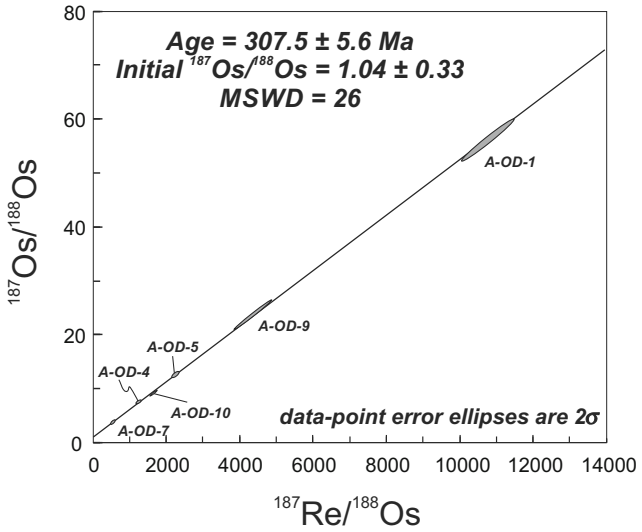

Fig. 6 Re–Os isochron diagram for six arsenopyrite samples from the Gustav orebody, Obří důl polymetallic skarn deposit

424 °C and only secondary fluid inclusions (T_h 228–262 °C, salinity up to 8 wt% NaCl equiv.) were found in garnet (grossular). No sulfide mineralization was reported from skarn at Garby Izerskie and documented silicification began at least at 410 °C (Fila-Wójcicka 2000). The quartz veinlets with the sulfide mineralization at the Obří důl deposit contain aqueous fluid inclusions with only small amounts of CO_2. They have mostly constant liquid/vapor ratio and a narrow range of T_h 324–358 °C with salinity in the range 4.0–8.8 wt% NaCl equiv. These values are similar to those reported from the Czarnów mineralized quartz veins (Mikulski et al. 2007). The eutectic temperature around − 34.5 °C indicates, except for NaCl, also the presence of Mg and Fe chlorides in the fluids. The formation of younger carbonate and quartz veinlets postdates the formation of both the Obří důl skarn mineral paragenesis and the major sulfide phase and is associated with low-temperature saline aqueous fluid inclusions (up to 8 wt% NaCl equiv., Na ± K ± Mg ± Fe chlorides) with T_h in the range 113–168 °C.

Multiple fluid sources constrained through C–O–Sr isotopic compositions

Isotopic investigations, particularly the stable isotopic compositions of C, O, H, and S, have been critically important for a

Table 4 Re–Os data for arsenopyrite from the Gustav orebody (Kovárna mining area, the Obří důl polymetallic skarn deposit)

Sample	Re (ppb)	2σ	Total Os (ppt)	^{187}Os (ppt)	2σ	$^{187}Re/^{188}Os$	2σ	$^{187}Os/^{188}Os$	2σ
A-OD-1	25.29	0.11	94.1	82.2	0.7	10,742	584	56.1	3.1
A-OD-4	5.396	0.024	41.3	19.2	0.1	1236	22	7.49	0.13
A-OD-5	7.001	0.031	39.3	23.6	0.3	2252	64	12.59	0.38
A-OD-7	2.349	0.011	32.0	9.2	0.07	520	14	3.74	0.1
A-OD-9	6.106	0.027	27.5	20.4	0.1	4360	382	23.65	2.07
A-OD-10	7.682	0.035	49.1	255	0.1	1647	77	9.21	0.43

documentation of the multiple fluid sources present in most large skarn systems (e.g., Shimazaki 1988; Bowman 1998; Meinert et al. 2003 and references therein).

Sulfur

Sulfur isotope studies on a variety of sulfide minerals (including pyrite, pyrrhotite, molybdenite, chalcopyrite, sphalerite, bornite, arsenopyrite, and galena) from skarn deposits indicate a very narrow range of $\delta^{34}S$ values, consistent with a homogeneous source of sulfur from magmatic fluids (e.g., Shimazaki and Yamamoto 1979; Shimazaki and Sakai 1984). This is in agreement with the observed $\delta^{34}S$ values found at the Obří důl deposit indicating a homogeneous sulfur source and dominantly reducing conditions during the formation of sulfides (i.e., low proportion of sulfate in the fluids). The source of sulfur is difficult to ascertain, since the background data defining the sulfur isotopic composition of the KJPC and the metamorphic series hosting the Obří důl skarn are unknown. Nevertheless, the whole range of sulfur isotope data (0.9 to 4.8‰) is in agreement with the range commonly observed in magmatic rocks of the Bohemian Massif (e.g., Bernard and Žák 1992). Unfortunately, the sulfur isotope thermometers are difficult to apply, since the observed sulfides are largely not in isotopic equilibrium and pyrrhotite–chalcopyrite fractionation is very steep (with respect to given analytical error) at high temperatures (cf. Kajiwara and Krouse 1971).

Carbon and oxygen in carbonates

The application of carbon and oxygen isotope analyses of carbonates became a routine method for the studies of both metamorphic decarbonization in calc–silicate rocks and metasomatic skarn-forming processes (e.g., Valley 1986 and references therein) applicable also for the skarn formation in the Bohemian Massif (Žák and Sztacho 1994; Drahota et al. 2005). The data provides clues to metamorphic decarbonization between the two theoretical end-members—a system continuously opened for CO_2 escape (Rayleigh volatilization) or decarbonization with a single-stage CO_2 escape (batch volatilization). Furthermore, carbonates isotopically equilibrate with, or formed from infiltrating, externally derived metasomatic fluids. Mathematical modeling can constrain the parameters of external fluid infiltration, i.e., define which parts of the mineral paragenesis were modified in a fluid-dominated system, and whether the fluid flow was pervasive or channelized (Baumgartner and Valley 2001).

At metamorphic temperatures, the escaping CO_2 has $\delta^{13}C$ and $\delta^{18}O$ values always higher than that of the residual rocks. Therefore, metamorphic decarbonization shifts the $\delta^{13}C$ and $\delta^{18}O$ of residual carbonate to lower values. Larger isotopic fractionations of $\delta^{13}C$ are generally produced during open system (Rayleigh) volatilization with continuous CO_2 escape and a low quantity of residual carbonate will yield very low $\delta^{13}C$ values. In contrast, the shift in $\delta^{18}O$ of the residual calc–silicate rocks is more restricted even under open-system behavior, since most oxygen in the system is always retained in the residual minerals. This so-called calc–silicate limit (Valley 1986) typically restricts the metamorphic coupled C–O isotopic fractionation observed in residual carbonate to a smaller change in $\delta^{18}O$, usually not exceeding 6‰. Larger shifts in the $\delta^{18}O$ values are typically observed in cases of external fluid infiltration and in fluid-dominated systems (e.g., Bowman et al. 1994).

The Obří důl skarn represents a complex case, since the rock sequence hosting the deposit was metamorphosed at least twice—by regional metamorphism and by contact metamorphism associated with the intrusion of the KJPC. Additionally, the un-metamorphosed limestone equivalents are not available and even the age of the whole sequence is poorly constrained. Other studies of skarns with polymetallic sulfide mineralization have shown that the rock sequences are commonly infiltrated and replaced by large volumes of externally derived fluids (Baumgartner and Valley 2001). The Izera–Kowary Unit hosting the Obří důl skarn is supposed to be of Cambrian or Lower Ordovician age (Oberc-Dziedzic et al. 2010), and therefore, the original limestone protoliths can have a $\delta^{13}C$–$\delta^{18}O$ composition as shown in Fig. 5a (estimated after Veizer et al. 1999). The C- and O-isotope shifts to the field of marbles and calc–silicate rocks are near the highest possible limit, which can be reached by "isochemical" bi-metasomatic exchange and fluid escape under high percentages of decarbonization. However, since these rocks are still rich in carbonate (see Table 3), the data must also reflect the isotopic exchange with external fluids, most likely during the regional metamorphism. The carbonates within skarn and calc–silicate rocks with sulfide mineralization create a negative array in C–O compositions (Fig. 5) in agreement with the observation that they contain a mixture of younger and primary calcite in the matrix. In detail, the carbonates in this group show large $\delta^{13}C$ shifts from the field of both hypothetical protolith limestones and the field of un-mineralized calc–silicate rocks. Thus, their composition is completely controlled by overprint by channelized metasomatic fluid flow, which is most probably related to the intrusion of the KJPC.

The carbonate veinlet crosscutting a marble shows extremely low $\delta^{18}O$ data (− 27.2‰) as a result of its formation from a low-$\delta^{18}O$ fluid of meteoric provenance at low temperatures, as also indicated by the temperature data of late fluid inclusions of the post-ore assemblage.

Strontium

There are several potential strontium sources in the study area. The primary $^{87}Sr/^{86}Sr$ composition of carbonate can be

estimated from the well-documented global evolution curve, applicable to marine carbonates: the $^{87}Sr/^{86}Sr$ value peaks at about 0.7092 during late Cambrian, drops towards a minimum of 0.7077 at the end of Ordovician, and again steeply increases in early Silurian (Denison et al. 1993; Veizer et al. 1999; McArthur et al. 2001). All analyzed samples have higher values, indicating that the Sr isotopic system is disturbed and cannot be used for stratigraphic considerations. The more radiogenic values could be connected with sedimentation within a closed basin, i.e., an environment not in equilibrium with the global ocean. However, the isotopic compositions of the Izera–Kowary mica schists and its (meta) sedimentary equivalents (Linnemann and Romer 2002; Fila-Wójcicka 2004; Oberc-Dziedzic et al. 2009) indicate a rather unevolved, mostly mafic island arc protolith with presumably unradiogenic Sr isotopic fingerprint. Correspondingly, the seawater $^{87}Sr/^{86}Sr$ isotopic composition formed by mixing of oceanic seawater and continent-derived Sr should be generally below 0.710. Another potential source of radiogenic Sr could be the KJPC and/or accompanying percolating fluids. However, available initial $^{87}Sr/^{86}Sr$ data for all uncontaminated granites are well below 0.7090 (Kryza et al. 2014). Finally, mica schist of the Izera–Kowary Unit can represent the Sr source. Although there is no data for its $^{87}Sr/^{86}Sr$ ratio, the bulk-rock Rb/Sr ratio reaches ~ 5 or even higher (e.g., Oberc-Dziedzic et al. 2009). Consequently, the time-integrated ingrowth of $^{87}Sr/^{86}Sr$ from the end of Ordovician until the KJPC intrusion should result in values higher than 0.730 for any realistic $^{87}Sr/^{86}Sr$ initial values and even higher for Rb-rich minerals such as biotite. It is thus very likely that the radiogenic Sr isotopic compositions of the Obří důl skarn carbonates are due to influx of Sr leached from surrounding mica schists, most probably by fluids mobilized by the nearby intrusion. This effect is most evident in case of the late carbonate veinlet (Fig. 5b).

Temporal and spatial evolution

The formation of a skarn deposit is a dynamic process (e.g., Meinert et al. 2005 and references therein). In most large skarn deposits, there is a transition from early/distal metamorphism producing hornfels, reaction skarn, and massive skarn to later/proximal metasomatism resulting in relatively coarse-grained ore-bearing skarn. Due to the strong temperature gradients and large fluid circulation cells caused by intrusion of magma (Salemink and Schuiling 1987), contact metamorphism can be considerably more complex than the simple model of isochemical recrystallization typically invoked for regional metamorphism.

The roughly tabular KJPC shows a prolonged history of successive, multi-stage magma emplacement during the Variscan orogeny. The pluton fabrics and inferred magmatic strain patterns do not record the early petrogenetic processes but are consistent with the granitic magmas having been emplaced as already homogenized phenocryst-bearing mushes into the shallow crust (Žák et al. 2013). For skarns related to plutons, there is a parallel relationship between the sequence of emplacement, crystallization, alteration, and cooling of the pluton and the corresponding metamorphism, metasomatism, and retrograde alteration in the surrounding rocks (Meinert 1983). The KJPC intrudes into a structure represented by Cambro–Ordovician orthogneiss to the north (Kröner et al. 2001; Oberc-Dziedzic et al. 2005, 2009) and Neoproterozoic–Lower Paleozoic metamorphic rocks dominated by phyllite and mica schist with subordinate lenses of orthogneiss and bimodal metavolcanic rocks to the south and east (Marheine et al. 1999; Winchester et al. 2003). The Obří důl skarn deposit is developed in the SE contact aureole of the KJPC, up to a few hundred meters from the granite intrusion. The surrounding metamorphic rock sequence clearly experienced several successive events:

i. Primary deposition of the sediments including limestone lenses in the Cambrian and Ordovician
ii. Cadomian metamorphism and magmatism resulting in the formation of rocks, which were converted to orthogneiss later during the Variscan events
iii. Variscan regional metamorphism
iv. Intrusion of the KJPC causing contact metamorphism and metasomatism of the adjacent rocks forming calc–silicate rocks and skarns
v. Formation of high-temperature sulfide mineralization genetically related to the intrusion of KJPC which postdates formation of the skarns and possibly related retrograde changes to amphibolite and epidote-rich assemblages
vi. Several late events, some of them probably significantly separated in time, such as formation of W–(Sn) impregnations, tectonic disturbance of the KJPC contact zone under brittle regime, recrystallization of some sulfides, formation of late-stage carbonate veinlets, and formation of low-temperature phases related to mineralization

The data obtained within this study bring new information especially on the (v) and (vi) phases of this multistage process. The spatial connection of polymetallic skarns with the contact of KJPC argues for skarn formation by metasomatism related to the Variscan magmatism.

The Re–Os age data for arsenopyrite from the Gustav orebody (307.5 ± 5.6 Ma; Fig. 6) are in agreement with the Re–Os age of molybdenite separated from the mineralized section of the Obří důl skarn (312.7 ± 1.4 Ma; Ackerman et al. 2017), single arsenopyrite Re–Os model ages in the range of 309–315 Ma for the nearby Au–As Czarnów deposit, and a molybdenite Re–Os age (312 ± 1 Ma) reported for the Kowary Fe–U–polymetallic deposit (Mikulski and Stein 2013). These age data clearly indicate that the formation of polymetallic

sulfide mineralization is chronologically related to the intrusion of the KJPC. The results are undistinguishable within error from U–Pb zircon ages from the part of KJPC spatially closest to the Obří důl deposit (312.5 ± 0.3 to 312.2 ± 0.3 Ma; CA–ID–TIMS; Kryza et al. 2014) and Re–Os molybdenite ages of 307 ± 2 and 309 ± 2 Ma from Fe–Cu–Mo–W mineralization related to the KJPC (Mayer et al. 2012). They are also similar to the Garby Izerskie skarn (302 Ma, Rb–Sr whole-rock; Fila-Wójcicka 2004) and accompanying hornfelsed schist (333 ± 4 Ma, Rb–Sr whole-rock; Fila-Wójcicka 2004), which is interpreted as the age of late-stage hydrothermal overprint of skarn. Our new age data also confirms the idea of Šrein and Šreinová (2000) who interpreted the pyrrhotite recrystallization at the Obří důl as a result of tectonic processes postdating the KJPC intrusion and formation of the sulfide ores.

The study of the metamorphic evolution of metabasites in the SE part of the KJPC showed that the peak metamorphic temperature of 615–640 °C and pressure of 7.3–8.2 kbar were preceded by an earlier stage (T = 370–550 °C, P = 2.8–6.2 kbar), while the final metamorphic episode took place at 450–550 °C and 2.5–4.8 kbar (Ilnicki 2011). Retrograde re-equilibration in greenschist/sub-greenschist facies at temperatures < 300–350 °C and pressures < 2.5–3.0 kbar) was partly related to hydrothermal activity around the KJPC, which is consistent with results of our fluid inclusion study on the main sulfide stage. However, our fluid inclusion study was not able to trace the evolution of fluids from the early, magmatic high-salinity type, to later less saline completely. Nevertheless, the participation of late low-$\delta^{18}O$ fluids is evidenced by some late calcite types in skarns and by very late, low-temperature calcite veinlets without any ore minerals.

Conclusions

Our mineralogical, geochemical, and isotopic study of the massive and impregnated sulfide mineralization and accompanying carbonate-bearing rocks from the Gustav orebody, a part of the Obří důl skarn deposit, resulted in the following findings:

1. The Gustav orebody consists dominantly of pyrrhotite and chalcopyrite which mainly replace silicate minerals (diopside). Arsenopyrite was found to be the oldest sulfide mineral. Minor ore minerals are represented by sphalerite, pyrite, marcasite, cassiterite, molybdenite, stokesite, native Bi, bismuthinite, galena, and S–Pb–Bi–Ag phases. The sulfide paragenesis clearly postdates formation of the pyroxene–garnet assemblage.
2. Fluid inclusion study revealed the existence of three types of paleofluids: (i) H_2O-type fluids in diopside with T_h = 387–424 °C and salinity up to 8 wt% NaCl equivalent, (ii) H_2O-type fluids with low CO_2 values in quartz veins with sulfide mineralization (minimum temperature of sulfide formation T_h = 324–358 °C, salinity 4.0–8.8 wt% NaCl equivalent, and indicated presence of Mg and Fe chlorides), and (iii) H_2O-type fluids in carbonate veins and younger quartz veins with T_h = 113–168 °C, salinity up to 8 wt% NaCl equivalent, and presence of K–Mg–Fe chlorides.
3. The sulfur isotopic composition of pyrrhotite, chalcopyrite, and arsenopyrite yields a very narrow range of $\delta^{34}S$ values (0.9–4.8‰), consistent with a source of sulfur from magmatic rocks of the Bohemian Massif.
4. Carbonates from mineralized skarn and calc–silicate rocks shows large shifts in $\delta^{18}O$ away from the field of both hypothetical protolith limestone and the field of un-mineralized calc–silicate rocks (carbonate $\delta^{18}O$ values ranging from − 13.4 to − 25.2‰ V-PDB), suggesting their total overprint by channelized metasomatic fluid flow, which is most probably related to the intrusion of the Krkonoše–Jizera Plutonic Complex (KJPC).
5. The strontium isotopic compositions of carbonate fractions generally correlate with both C and O isotopes. The least radiogenic sample ($^{87}Sr/^{86}Sr$ = 0.7098) has also the highest $\delta^{13}C$ and $\delta^{18}O$ values, closest to the presumed marine carbonate composition. The other more radiogenic samples with $^{87}Sr/^{86}Sr$ up to 0.7190 in a late-stage carbonate veinlet most likely reflect a contribution of radiogenic Sr leached from surrounding mica schists by fluids mobilized by the intrusion of the KJPC.
6. The Re–Os age of arsenopyrite (307.5 ± 5.6 Ma) is chronologically closely related to the later stages of the KJPC intrusion and evolution.
7. The homogenization temperature range (324–358 °C), derived from the fluid inclusion study of the main sulfide stage at the Gustav orebody, is consistent with retrograde re-equilibration of the surrounding rocks under greenschist/sub-greenschist facies conditions (T < 300–350 °C, P < 2.5–3.0 kbar) which was partly related to hydrothermal activity around the KJPC.

Acknowledgements This study is a contribution to the GAČR project 13-15390S to LA and JP. We thank Z. Lněničková, Bohuslava Čejková and Ivana Jačková (Czech Geological Survey) for the sulfur, carbon and oxygen isotope analysis, R. Škoda (Czech Geological Survey/Masaryk University) for the EMPA, J. Rohovec for the ICP-OES measurements, and J. Kallistová (Czech Academy of Sciences) for the X-ray analyses. This is also a contribution to the Scientific Programme RVO67985831 of the Institute of Geology of the CAS and the Strategic Research Plan of the Czech Geological Survey (2016–2020). We thank Zdeněk Pertold and Stanislav Mikulski for the comprehensive reviews which improved the manuscript significantly and Bernd Lehmann for careful handling.

References

Ackerman L, Haluzová E, Creaser RA, Pašava J, Veselovský F, Breiter K, Erban V, Drábek M (2017) Temporal evolution of mineralization events in the Bohemian Massif inferred from the Re-Os geochronology of molybdenite. Mineral Deposita 52:651–662

Aleksandrowski P, Mazur S (2002) Collage tectonics in the northeasternmost part of the Variscan Belt: the Sudetes, Bohemian Massif. In: Winchester JA, Pharaoh TC, Vernieres J (eds) Geological Society Special Publication. Geological Society of London, London, pp 237–277

Awdankiewicz M (2007) Late Palaeozoic lamprophyres and associated mafic subvolcanic rocks of the Sudetes (SW Poland): petrology, geochemistry and petrogenesis. Geol Sudet 39:11–97

Baumgartner LP, Valley JW (2001) Stable isotope transport and contact metamorphic fluid flow. Rev Mineral Geochem 43:415–467

Bernard JH, Hyršl J (2013) Minerals and their localities. Granit Publishing, Prague

Bernard JH, Pouba Z (1986) Rudní ložiska a metalogeneze československé části Českého masívu. Ústřední Ústav Geologický, Praha

Bernard JH, Žák K (1992) Stable isotope study of Variscan vein Pb-Zn-Ag mineralization of the Bohemian Massif. Explor Min Geol 1:81–84

Białek D, Kryza R, Oberc-Dziedzic T, Pin C (2014) Cambrian Zawidów granodiorites in the Cadomian Lusatian Massif (Central European Variscides): what do the SHRIMP zircon ages mean? J Geosci 59:313–326

Birck JL, Barman MR, Capmas F (1997) Re-Os isotopic measurements at the femtomole level in natural samples. Geostand Newslett J Geostand Geoanal 20:19–27

Bodnar RJ, Vityk MO (1995) Interpretation of the microthermometric data for H2O-NaCl fluid inclusions. In: De Vivo B, Frezzotti ML (eds) Fluid inclusions in minerals: Methods and applications. Virginia Polytechnic Institute, Blacksburg, pp 117–130

Borkowska M (1966) Petrografia granitu Karkonoszy. Geol Sudetica 2:7–120

Bowman JR (1998) Stable-isotope systematics of skarns. In: Lentz DR (ed) Mineralized Intrusion-related Skarn Systems. Mineralogical Association of Canada, Quebec City, pp 99–145

Bowman JR, Willett SD, Cook SJ (1994) Oxygen isotope transport and exchange during fluid flow: one-dimensional models and applications. Am J Sci 294:1–55

Breiter K, Förster HJ, Seltmann R (1999) Variscan silicic magmatism and related tin-tungsten mineralization in the Erzgebirge-Slavkovsky les metallogenic province. Mineral Deposita 34:505–521

Bubal J (2013) Geochemie a vznik skarnů Českého masivu. Unpublished MSc. Thesis, Charles University

Bubal J, Dolejš D (2013) Magnetite chemistry in skarns of the Bohemian Massif: evaluating competing effects of protolith inheritance, crystal chemistry, fluid composition and pressure-temperature conditions. In: Jonsson E (ed) Mineral deposit research for a high-tech world, proceedings of the 12th SGA Meeting. Society for Geology Applied to Mineral Deposits, Uppsala, pp 264–267

Buschmann B, Nasdala L, Jonas P, Linnemann U, Gemlich M (2001) Shrimp U-Pb dating of tuff-derived and detrital zircons from Cadomian marginal basin fragments (Neoproterozoic) in the northeastern Saxothuringian Zone (Germany). Neu Jb Geol Paläontol, Mh 6:321–342

Buschmann B, Elicki O, Jonas P (2006) The Cadomian unconformity in the Saxo-Thuringian Zone, Germany: palaeogeographic affinities of Ediacaran (terminal Neoproterozoic) and Cambrian strata. Precambrian Res 147:387–403. https://doi.org/10.1016/j.precamres.2006.01.023

Chrt J, Bolduan H (1966) Die postmagmatische Mineralisation des Westteils der Böhmischen Masse. Sbor Geol Věd, Lož Geol 8:113–192

Creaser RA, Papanastassiou DA, Wasserburg GJ (1991) Negative thermal ion mass spectrometry of osmium, rhenium, and iridium. Geochim Cosmochim Acta 55:397–401

Davis DW, Lowenstein TM, Spencer RJ (1990) Melting behavior of fluid inclusions in laboratory-grown halite crystals in the systems NaCl-H2O, NaCl-KCl-H2O, NaCl-MgCl2-H2O, and NaCl-CaCl2-H2O. Geochim Cosmochim Acta 54:591–601

Denison RE, Koepnick RB, Fletcher A, Dahl DA, Baker MC (1993) Reevaluation of early Oligocene, Eocene, and Paleocene seawater strontium isotope ratios using outcrop samples from the U.S. Gulf Coast. Paleoceanography 8:101–126

Drahota P, Pertold Z, Pudilová M (2005) Three types of skarn in the northern part of the Moldanubian Zone, Bohemian Massif—implications for their origin. J Czech Geol Soc 50:19–33

Einaudi MT, Burt DM (1982) Introduction—terminology, classification, and composition of skarn deposits. Econ Geol 77:745–754

Einaudi MT, Meinert LD, Newberry RJ (1981) Skarn deposits. In: Skinner BJ (ed) Economic geology, seventy-fifth anniversary volume (1905–1980). Economic Geology, Littleton, pp 317–391

Fettes D, Desmonds J (2007) Metamorphic Rocks. A classification and glossary of terms. Cambridge University Press, Cambridge

Fila-Wójcicka E (2000) Petrogenesis of the calc-silicate skarns from Garby Izerskie, Karkonosze-Izera block. Acta Geol Pol 50:221–222

Fila-Wójcicka E (2004) Rb-Sr isotope studies in the Garby Izerskie Zone—evidence for the Karkonosze intrusion activity. Mineral Soc Pol – Spec Pap 24:153–156

Finger F, Gerdes A, René M, Riegler G (2009) The Saxo-Danubian Granite Belt: magmatic response to post-collisional delamination of mantle lithosphere below the southwestern sector of the Bohemian Massif (Variscan orogeny). Geol Carpath 60:205–212

Franke W (1995) Exhumation of HP-rocks in the Saxo-Thuringian Belt: back-arc extension? J Czech Geol Soc 40:8–9

Franke W (1989) Variscan plate tectonics in Central Europe—current ideas and open questions. Tectonophysics 169:221–228

Grinenko VA (1962) The preparation of sulphur dioxide for isotopic analysis. Zhurnal Neorg Khimii 7:478–483

Hladil J, Patočka F, Kachlík V (2003) Metamorphosed carbonates of Krkonoše Mountains and Paleozoic evolution of the Sudetic terranes (NE Bohemia, Czech Republic). Geol Carpath 54:281–297

Holmes A (1920) The nomenclature of petrology, with references to selected literature. Murby & Co, London

Hoth K, Lorenc MW (1966) Die skarnhöffigen Horizonte des westlichen Erzgebirges. Andean Geol 15:769–799

Ilnicki S (2011) Variscan prograde P-T evolution and contact metamorphism in metabasites from the Sowia Dolina, Karkonosze–Izera massif, SW Poland. Mineral Mag 75:185–212

Jamtveit B, Anderson T (1993) Contact metamorphism of layered shale-carbonate sequences in the Oslo rift: III. The nature of the skarn-forming fluids. Econ Geol 88:1830–1849

Kachlík V, Patočka F (1998) Cambrian/Ordovician intracontinental rifting and Devonian closure of the rifting generated basins in the Bohemian Massif realms. Acta Univ Carol Geol 42:433–441

Kajiwara Y, Krouse HR (1971) Sulfur isotope partitioning in metallic sulfide systems. Can J Earth Sci 8:1397–1408

Kemnitz H, Romer RL, Oncken O (2002) Gondwana break-up and the northern margin of the Saxothuringian Belt (Variscides of Central Europe). Int J Earth Sci 91:240–259

Kerr A, Selby D (2011) The timing of epigenetic gold mineralization on the Baie Verte Peninsula, Newfoundland, Canada: new evidence from Re–Os pyrite geochronology. Mineral Deposita 47:325–337. https://doi.org/10.1007/s00126-011-0375-2

Klápová H, Konopásek J, Schulmann K (1998) Eclogites from the Czech part of the Erzgebirge: multi-stage metamorphic and structural evolution. J Geol Soc Lond 155:567–583

Klomínský J, Sattran V (1963) Entstehungsgeschichte der Skarne im mittleren Teil von Krušné hory (Erzgebirge). Věst Úst Ústav Geol 38:341–345

Kosmatt F (1927) Gliederung des varistischen Gebirgsbaues. Abhandlungen des Sächsischen Geol Landesamtes 1:1–39

Koutek J (1950) The deposit of magnetite of skarn type at Vlastějovice in the Sázava Basin (Eastern Bohemia). Bull Int Acad Tchéque Sci 27:1–17

Kröner U, Romer RL (2010) The Saxo-Thuringian Zone—tip of the Armorican Spur and part of the Gondwana plate. In: Linnemann U, Romer RL (eds) Pre-Mesozoic geology of Saxo-Thuringia—from the Cadomian active margin to the Variscan Orogen. Schweizerbart, Stuttgart, pp 371–394

Kröner A, Hegner E, Hammer J, Haase G, Bielicki KH, Krauss M, Eidam J (1994) Geochronology and Nd-Sr systematics of Lusatian granitoids: significance for the evolution of the Variscan Orogen in east-central Europe. Geol Rundsch 83:357–376

Kröner A, Jaeckel P, Hegner E, Opletal M (2001) Single zircon ages and whole-rock Nd isotopic systematics of early Palaeozoic granitoid gneisses from the Czech and Polish Sudetes (Jizerské hory, Krkonoše Mountains and Orlice-Sněžník Complex). Int J Earth Sci 90:304–324

Kryza R, Schaltegger U, Oberc-Dziedzic T, Pin C, Ovtcharova M (2014) Geochronology of a composite granitoid pluton: a high-precision ID-TIMS U–Pb zircon study of the Variscan Karkonosze Granite (SW Poland). Int J Earth Sci 103:683–696

Kurfiřt R, Tásler R (2014) Copper and arsenic production by the Riesenhain Works in Pec pod Sněžkou in the years 1828–1868. Opera Concortica 51:69–84

Kwak TAP (1986) Fluid inclusions in skarns (carbonate replacement deposits). J Metamorph Geol 4:363–384

Linnemann U, Romer RL (2002) The Cadomian Orogeny in Saxo-Thuringia, Germany: geochemical and Nd-Sr-Pb isotopic characterization of marginal basins with constraints to geotectonic setting and provenance. Tectonophysics 352:33–64

Linnemann U, Gehmlich M, Tikhomirova M, Buschmann B, Nasdala L, Jonas P, Lutzer H, Bombach K (2000) From Cadomian subduction to Early Palaeozoic rifting: the evolution of Saxo-Thuringia at the margin of Gondwana in the light of single zircon geochronology and basin development (Central European Variscides, Germany). Geol Soc Lond Spec Publ 179:131–153

Linnemann U, McNaughton NJ, Romer RL, Gemlich M, Drost K, Tonk C (2004) West African provenance for Saxo-Thuringia (Bohemian Massif): did Armorica ever leave pre-Pangean Gondwana? U/Pb-SHRIMP zircon evidence and the Nd-isotopic record. Int J Earth Sci 93:683–705

Linnemann U, Gerdes A, Drost K, Buschmann B (2007) The evolution of the Rheic Ocean: from Avalonian-Cadomian active margin to Alleghenian-Variscan Collision. Geol Soc Am Spec Pap 423:61–96

Linnemann U, D'Lemos R, Drost K, Jeffries T, Gerdes A, Romer RL, Samson SD, Strachan RA (2008a) Cadomian tectonics. In: McCann T (ed) Geology of Central Europe. Geological Society of London, London, pp 103–154

Linnemann U, Pereira F, Jeffries TE, Drost K, Gerdes A (2008b) The Cadomian Orogeny and the opening of the Rheic Ocean: the diacrony of geotectonic processes constrained by LA-ICP-MS U–Pb zircon dating (Ossa-Morena and Saxo-Thuringian Zones, Iberian and Bohemian Massifs). Tectonophysics 461:21–43

Makovicky E (2006) Crystal structures of sulfides and other chalcogenides. Rev Mineral Geochem 61:7–125

Marheine D, Kachlík V, Patočka F, Maluski H (1999) The Palaeozoic polyphase tectono-thermal record in the Krkonoše–Jizera Crystalline Unit (West Sudetes, Czech Republic). Andean Geol 9: 133–135

Matte P, Maluski H, Rajlich P, Franke W (1990) Terrane boundaries in the Bohemian Massif: result of large-scale Variscan shearing. Tectonophysics 177:151–170

Mayer W, Creaser R, Mochnacka K, Pieczka A (2012) Isotopic Re-Os age of molybdenite from the Szklarska Poręba Huta Quarry (Karkonosze, SW Poland). Geol Q 56:505–512

Mazur S, Aleksandrowski P, Turniak K, Awdankiewicz M (2007) Geology, tectonic evolution and Late Palaeozoic magmatism of Sudetes: an overview. In: Kozlowski A, Wiszniewska J (eds) Granitoids in Poland. Faculty of Geology of The Warsaw University, Warszaw, pp 59–87

Mazur S, Turniak K, Szczepanski J, McNaughton NJ (2015) Vestiges of Saxothuringian crust in the Central Sudetes, Bohemian Massif: zircon evidence of a recycled subducted slab provenance. Gondwana Res 27:825–839

McArthur JM, Howarth RJ, Bailey TR (2001) Strontium isotope stratigraphy: LOWESS version 3: best fit to the marine Sr-isotope curve for 0–509 Ma and accompanying look-up table for deriving numerical age. J Geol 109:155–170

McCrea JM (1950) On the isotope chemistry of carbonates and a paleotemperature scale. J Chem Phys 18:849–857

Meinert LD (1983) Variability of skarn deposits—guides to exploration. In: Boardman SJ (ed) Revolution in the Earth Sciences: advances in the Past Half-Century. Kendall-Hunt, Dubuque, pp 301–316

Meinert LD (1992) Skarns and skarn deposits. Geosci Can 19:145–162

Meinert LD, Dipple GM, Nicolescu S (2005) World Skarn Deposits. Econ Geol 100th Anni: 299–336

Meinert LD, Hedenquist JW, Satoh H, Matsuhisa Y (2003) Formation of anhydrous and hydrous skarn in Cu-Au ore deposits by magmatic fluids. Econ Geol 98:147–156

Mikulski SZ, Kozlowski A, Speczik S (2007) Fluid inclusion study of gold-bearing quartz-sulfide veins and cassiterite from the Czarnów As deposit ore (SW Poland). In: Colin A (ed) Digging Deeper, Proceedings of 9th Biennial SGA Meeting, Vol 1, In: Andrew, C.J., et al. (Eds.), Digging Deeper. Proceedings of the 9th SGA Biennal Meeting, Dublin. Springer Verlag, Berlin, pp 805–808

Mikulski SZ (2010) The characteristic and genesis of the gold-bearing arsenic polymetallic mineralization in the Czarnów deposit (West Sudetes). Biul - Panstw Inst Geol 439:303–320

Mikulski SZ, Stein HJ (2013) Re-Os ages for sulphides from the (gold-)polymetallic deposits in the eastern metamorphic cover of the Karkonosze Massif (SW Poland). In: Jonsson E et al (eds) Mineral Deposits Research for a High-Tech World, Proceedings of 12th Biennial SGA Meeting, vol 1. Elanders, Sverige AB, pp 217–221

Mikulski SZ, Speczik S (2016) The auriferous ore mineralisation and its zonal distribution around the Variscan Klodzko–Zloty Stok granitoid pluton in the Sudetes (SW Poland)—an overview. Geol Q 60: 650–674

Mochnacka K, Pošmourný K (1981) Metallogenetic characteristics of the Palaeozoic and pre-Palaeozoic formations of the northern part of the Bohemian Massif (Krkonoše-Jizerské hory region). Čas Mineral Geol 26:29–43

Mochnacka K, Oberc-Dziedzic T, Mayer W, Pieczka A, Góralski M (2009) New insights into the mineralization of the Czarnów ore deposit (West Sudetes, Poland). Geol Sudetica 41:43–56

Mochnacka K, Oberc-Dziedzic T, Mayer W, Pieczka A (2015) Ore mineralization related to geological evolution of the Karkonosze-Izera Massif (the sudetes, Poland)—Towards a model. Ore Geol Rev 64: 215–238

Morelli R, Creaser RA, Seltmann R, Stuart FM, Selby D, Graupner T (2007) Age and source constraints for the giant Muruntau gold deposit, Uzbekistan, from coupled Re-Os-He isotopes in arsenopyrite. Geology 35:795–798

Morelli RM, Bell CC, Creaser RA, Simonetti A (2010) Constraints on the genesis of gold mineralization at the Homestake Gold Deposit, Black Hills, South Dakota from rhenium–osmium sulfide geochronology. Mineral Deposita 45:461–480

Němec D (1964) Skarny županovické oblasti. Sb Geol Věd, Lož Geol 3: 43–107

Novák F (1964) Vazba cínu a wolframu na ložisku Obří důl v Krkonoších. Věst Úst Ústav Geol 39:127–132

Oberc-Dziedzic T, Pin C, Kryza R (2005) Early Palaeozoic crustal melting in an extensional setting: petrological and Sm–Nd evidence from the Izera granite-gneisses, Polish Sudetes. Int J Earth Sci 94:354–368

Oberc-Dziedzic T, Kryza R, Pin C, Mochnacka K, Larionov A (2009) The orthogneiss and schist complex of the Karkonosze-Izera Massif (Sudetes, SW Poland): U–Pb SHRIMP zircon ages, Nd-isotope systematics and protoliths. Geol Sudet 41:2–24

Oberc-Dziedzic T, Kryza R, Mochnacka K, Larionov A (2010) Ordovician passive continental margin magmatism in the Central-European Variscides: U–Pb zircon data from the SE part of the Karkonosze–Izera Massif, Sudetes, SW Poland. Int J Earth Sci 99:27–46

Pašava J, Kříbek B, Dobeš P, Vavřín I, Žák K, Delian F, Tao Z, Boiron MC (2003) Tin-polymetallic sulfide deposits in the eastern part of the Dachang tin field (South China) and the role of black shales in their origin. Mineral Deposita 38:39–66

Pašava J, Veselovský F, Drábek M, Svojtka M, Pour O, Klomínský J, Škoda R, Ďurišová J, Ackerman L, Halodová P, Haluzová E (2015) Molybdenite–tungstenite association in the tungsten-bearing topaz greisen at Vítkov (Krkonoše–Jizera Crystalline Complex, Bohemian Massif): Indication of changes in physico-chemical conditions in mineralizing system. J Geosci (Czech Republic)

Pašava J, Svojtka M, Veselovský F, Ďurišová J, Ackerman L, Pour O, Drábek M, Halodová P, Haluzová E (2016a) Laser ablation ICP-MS study of trace element chemistry in molybdenite—an important tool for identification of different types of mineralization. Ore Geol Rev 72:874–895

Pašava J, Veselovský F, Dobeš P, Haluzová E, Ackerman L, Tásler R (2016b) New mineralogical, fluid inclusion and sulfur isotope data of ores from the Obří důl skarn-type deposit (Bohemian Massif). Geosci Res Reports 49:47–52

Pertold Z, Kopecký L (1979) Vznik ložiska Obří důl a problém „polymetalických skarnů" Krkonoš. In: Sborník 22. konference Československé společnosti pro Mineralogii a Geologii. Geoindustria, Praha, pp 235–241

Pertold Z, Pouba Z (1982) Prävariszische Mineralisationen der peripheren Zone des Böhmischen Massivs (ČSSR). Z Angew Geol 28:366–370

Pertold Z, Pertoldová J, Pudilová M (1997) Metamorphic history of skarns in the Gföhl unit, Moldanubicum, Bohemian Massif, and implications for their origin. Acta Univ Carol Geol 41:157–166

Pertoldová J, Košulicová M, Verner K, Žáčková E, Pertold Z, Konopásek J, Veselovský F, Košler J (2014) Geochronology and petrology of pyroxene-garnet skarns (eastern Bohemian Massif): implications for the source and evolution of the Variscan continental crust. J Geosci 59:367–388

Pin C, Gannoun A, Dupont A (2014) Rapid, simultaneous separation of Sr, Pb, and Nd by extraction chromatography prior to isotope ratios determination by TIMS and MC-ICP-MS. J Anal At Spectrom 29: 1858–1870

Pošmourný K (1982) Stratiform iron ores in the crystalline of the north-east part of the Bohemian Massif (Krkonoše Mts., Železný Brod area, Orlické hory Mts.) J Geol Sci Econ Geol Mineral 23:125–170

Poty B, Leroy J, Jachimowicz L (1976) Un nouvel appareil pour la mesure des temperatures sous le microscope: L'installation de microthermometrie Chaixmeca. Bull Soc Fr Minéral Cristallogr 99:182–186

Pouba Z, Sattran V (1966) Problémy metalogeneze Českého masivu. Sb Geol Věd, Lož Geol 8:17–26

Reh H (1932) Beitrag zur Kenntnis der erzgebirgischen Erzlager. Neu Jb Mineral Geol Paläont Abh 65:1–86

Roedder E (1984) Fluid inclusions. Rev Mineral 12, Mineral Soc Amer, 644 pp

Romer RL, Thomas R, Stein HJ, Rhede D (2007) Dating multiply overprinted Sn-mineralized granites—examples from the Erzgebirge, Germany. Mineral Deposita 42:337–359

Salemink J, Schuiling RD (1987) A two-stage, transient heat and mass transfer model for the granodiorite intrusion at Seriphos, Greece, and the associated formation of contact metasomatic skarn and Fe-ore deposits. NATO Adv Study Institutes Ser C - Math Phys Sci 218:547–575

Shimazaki M (1988) Oxygen, carbon and sulfur isotope study of skarn deposits in Japan. In: Zachrisson E (ed) Proceedings of the 7th Quadrennial IAGOD Symposium. Schweizerbart'sche Verlagsbuchhandlung, Stuttgart, pp 375–381

Shimazaki M, Yamamoto M (1979) Sulfur isotope ratios of some Japanese skarn deposits. Geochem J 13:261–268

Shimazaki M, Sakai H (1984) Regional variation of sulfur isotope composition of skarn deposits in the westernmost part of the Inner zone of Southwest Japan. Min Geol 34:419–424

Shirey SB, Walker RJ (1995) Carius tube digestion for low-blank rhenium-osmium analyses. Anal Chim Acta 67:2136–2141

Schulmann K, Konopásek J, Janoušek V, Lexa O, Lardeaux JM, Edel JB, Štípská P, Ulrich S (2009) An andean type Palaeozoic convergence in the Bohemian Massif. Compt Rendus Geosci 341:266–286

Stein H, Morgan JW, Scherstén A (2000) Re-Os dating of low-level highly radiogenic (LLHR) sulfides: the Harnäs gold deposit, southwest Sweden, records continental-scale tectonic events. Econ Geol 95:1657–1671

Šrein V, Šreinová B (2000) Mineralogy of the skarns of the Bohemian part of the western and central Krušné hory mountains. Acta Mont A17:67–108

Tásler R (2012) A list of the existing mines and surficial mining landforms and an overview of the history of polymetallic deposit mining and present explorations in the Obří důl valley (Eastern Krkonoše Mts). Opera Concortia 49:31–54

Tichomirova M (2002) Zircon inheritance in diatexite granodiorites and its consequence on geochronology—a case study in Lusatia and the Erzgebirge (Saxo-Thuringia, eastern Germany). Chem Geol 191: 209–224

Valley JW (1986) Stable isotope geochemistry of metamorphic rocks. Rev Mineral 16:445–489

Veizer J, Ala D, Azmy K, Bruckschen P, Buhl D, Bruhn F, Carden Giles AF, Diener A, Ebneth S, Godderis Y, Jasper T, Korte C, Pawellek F, Podlaha OG, Strauss H (1999) $^{87}Sr/^{86}Sr$, $\delta^{13}C$ and $\delta^{18}O$ evolution of Phanerozoic seawater. Chem Geol 161:59–88

Völkening J, Walczyk T, Heumann KG (1991) Osmium isotope ratio determinations by negative thermal ionization mass spectrometry. Int J Mass Spectrom Ion Process 105:147–159

Wilkinson JJ (2001) Fluid inclusions in hydrothermal ore deposits. Lithos 55:229–272

Winchester JA, Patočka F, Kachlík V, Melzer M, Nawakowski C, Crowley QG, Loyd PA (2003) Geochemical discrimination of metasedimentary sequences in the Krkonoše-Jizera terrane (West Sudetes, Bohemian Massif): paleotectonic and stratigraphic constraints. Geol Carpath 54:267–280

Žáček V (2007) Potassian hastingsite and potassic hastingsite from garnet–hedenbergite skarn at Vlastějovice, Czech Republic. Neues Jb Mineral Abh 184:161–168

Žák J, Klomínský J (2007) Magmatic structures in the Krkonoše-Jizera Plutonic Complex, Bohemian Massif: evidence for localized multiphase flow and small-scale thermal-mechanical instabilities in a granitic magma chamber. J Volcanol Geotherm Res 164:254–267

Žák J, Verner K, Sláma J, Kachlík V, Chlupáčová M (2013) Multistage magma emplacement and progressive strain accumulation in the shallow-level Krkonoše-Jizera plutonic complex, Bohemian Massif. Tectonics 32:1493–1512

Žák K, Sztacho P (1994) Marbles, calc-silicate rocks and skarns of the Moldanubian Unit (Bohemian Massif): carbon and oxygen isotope and fluid inclusion constraints on their formation conditions. In: Nishiyama T, Fisher GW (eds) Proceedings 29th International Geological Congress. VSP International Science Publishers, Zeist, pp 39–49